



**HAL**  
open science

## **Deciphering transcriptomic and metabolomic wood responses to grapevine trunk diseases-associated fungi**

Ana Romeo-Oliván, Justine Chervin, Coralie Breton, Virginie Puech Pagès, Sylvie Fournier, Guillaume Marti, Olivier Rodrigues, Jean Daydé, Bernard Dumas, Alban Jacques

### ► **To cite this version:**

Ana Romeo-Oliván, Justine Chervin, Coralie Breton, Virginie Puech Pagès, Sylvie Fournier, et al.. Deciphering transcriptomic and metabolomic wood responses to grapevine trunk diseases-associated fungi. *PhytoFrontiers*, 2024, 10.1094/PHYTOFR-10-23-0132-R . hal-04551710

**HAL Id: hal-04551710**

**<https://hal.science/hal-04551710>**

Submitted on 18 Apr 2024

**HAL** is a multi-disciplinary open access archive for the deposit and dissemination of scientific research documents, whether they are published or not. The documents may come from teaching and research institutions in France or abroad, or from public or private research centers.

L'archive ouverte pluridisciplinaire **HAL**, est destinée au dépôt et à la diffusion de documents scientifiques de niveau recherche, publiés ou non, émanant des établissements d'enseignement et de recherche français ou étrangers, des laboratoires publics ou privés.

## **Deciphering transcriptomic and metabolomic wood responses to grapevine trunk diseases-associated fungi**

Ana Romeo-Oliván<sup>1, \*</sup>, Justine Chervin<sup>2,3,4, \*</sup>, Coralie Breton<sup>1</sup>, Virginie Puech-Pagès<sup>2,3,4</sup>, Sylvie Fournier<sup>2,3,4</sup>, Guillaume Marti<sup>2,3,4</sup>, Olivier Rodrigues<sup>1</sup>, Jean Daydé<sup>1</sup>, Bernard Dumas<sup>2</sup> and Alban Jacques<sup>1</sup>.

<sup>1</sup> *Unité de Recherche Physiologie, Pathologie, et Génétique Végétales (PPGV), INP PURPAN, Université de Toulouse, France.*

<sup>2</sup> *Laboratoire de Recherche en Sciences Végétales, Université de Toulouse, CNRS, UPS, Toulouse INP, France*

<sup>3</sup> *Metatoul-AgromiX platform, MetaboHUB, National Infrastructure for Metabolomics and Fluxomics, LRSV, Université de Toulouse, CNRS, UPS, Toulouse INP, France*

<sup>4</sup> *MetaboHUB-MetaToul, National Infrastructure of Metabolomics and Fluxomics, Toulouse, 31077, France*

\* These authors contributed equally to this work.

Corresponding author: A. Romeo-Oliván; Email: ana.romeo-olivan@purpan.fr

**Funding :** French National Infrastructure for Metabolomics and Fluxomics, Grant MetaboHUB-ANR-11-INBS-0010, and the PSPC SOLSTICE Project (SOLutionS pour des Traitements Intégrés dans une Conduite Environnementale) funded by the French state (Programme d'Investissements d'Avenir).

**Abstract**

Esca is one of the main grapevine trunk diseases affecting vineyards worldwide. *Phaeoacremonium minimum* and *Phaeoconiella chlamydospora* are thought to be two of the main causal agents of this disease. However, the molecular mechanisms underlying plant defense responses in the grapevine trunk against esca-associated pathogens are poorly understood. To provide a first glimpse on the trunk responses to *P. minimum* and *P. chlamydospora*, transcriptomic and metabolomic analyses were performed to compare and contrast host responses to these pathogens. Transcriptomic analysis revealed different gene expression reprogramming in the trunk in response to each fungus. Main significant differences were found among genes associated with Secondary Metabolism, Signaling and Hormone Signaling. An untargeted liquid chromatography–high resolution mass spectrometry metabolomic approach performed 3 weeks after inoculation was used and dereplication mainly highlighted flavonoids and stilbenes as plant defense metabolites in the infected trunk. Some metabolites were overproduced with both fungi, but specific responses were also observed. Particularly, a lipophilic flavonoid cluster was emphasized after *P. minimum* inoculation. The assessment of fungal infection 6 wpi showed a higher number of copies of *P. minimum* than *P. chlamydospora*. This dissimilarity in the level of colonization could be linked somehow to the metabolomic responses observed. Our results reveal both different gene expression reprogramming and metabolomic specific signatures depending on the wood pathogen. Altogether, these observations suggest that grapevine trunk can differently perceive and respond to *P. minimum* and *P. chlamydospora*.

**Keywords:** Esca, *P. minimum*, *P. chlamydospora*, transcriptomics, metabolomics, trunk defense responses.

## Introduction

Grapevine trunk diseases (GTD) are a group of destructive disorders caused by fungal pathogens that attack woody tissues and colonize grapevine xylem vessels (Fontaine et al., 2016). Esca is one of the main grapevine trunk diseases affecting vineyards worldwide. The main species associated with the esca disease are *Phaeoconiella chlamydospora*, *Phaeoacremonium minimum*, *Phaeoacremonium* spp. and diverse Basidiomycetes, such as *Fomitiporia mediterranea* (Larignon and Dubos, 1997; Bertsch et al., 2013). Symptoms in the aerial parts of the vine appear years after the infection and vary depending on the pathogens infecting the plant, the age and the physiological status of the vine and the environmental conditions. Moreover, infected vines may not present foliar symptoms every year (Guerin-Dubrana et al., 2019). Therefore, esca is a complex and still poorly understood disease. To date, there is no completely effective cure (Gramaje et al., 2009, 2018; Mondello et al., 2018) and every cultivated variety of *Vitis vinifera* is sensible to this disease (Bruez et al., 2013). A better understanding of the mechanisms underlying the infection might be essential to develop alternative and effective solutions to this disease.

Historically, defense responses in woody tissues have been described as non-pathogen-dependent but as generic responses (Shigo and Marx, 1977; Blanchette and Biggs, 1992). Recent pieces of evidence suggest that pathogen attack may in fact activate specific molecular mechanisms in the trunk depending on the infecting pathogen. For instance, Munkvold and Marois (1995) reported that the inoculation of *Eutypa lata*, the causal agent of Eutypa dieback, induced the accumulation of suberin in the zone of infection. Czermel et al. (2015) noticed a reduction on the starch content after the inoculation of *Neofusicoccum parvum*, the causal agent of the black dead arm. Several differences were noted between infections with different esca-related pathogens. The infection with *P. chlamydospora* leads to the formation of a

longitudinal section brown and a black streak (Lorena et al., 2001; Pouzoulet et al., 2013), which has never been observed after the inoculation of *P. minimum*. Moreover, several studies reported that *P. chlamydospora* interferes with wound healing (Pierron et al., 2016), which has never been reported for *P. minimum*.

The study of the esca-grapevine pathosystem is quite complicated. Different molecular approaches have been developed to explore the molecular mechanisms underlying defense responses on cellular cultures (Lima et al., 2012; Stempien et al., 2018), green stems (Spagnolo et al., 2012; Gonçalves et al., 2019), in leaves from symptomatic vines (Czemmel et al., 2015; Magnin-Robert et al., 2017; Goufo et al., 2019, 2021; Lemaitre-Guillier et al., 2021) or in artificially inoculated wood (Pierron et al., 2016; Massonnet et al., 2017; Labois et al., 2020; Galarneau et al., 2021). This latter method has provided valuable information concerning the early stages of fungal colonization in woody tissues (Pierron et al., 2015a). However, the study of molecular responses in the earliest stages of fungal infection present some difficulties, since the mechanical stress inflicted by the wound changes the expression of a large number of genes in the first 24h-48h hours (Pierron et al., 2016; Massonnet et al., 2017).

High throughput (-omics) technologies represent a good tool to deeply investigate plant-pathogen interactions. In the case of GTD, many metabolomic studies were performed on the leaf metabolome (Gimeno-Gilles et al., 2009; Lima et al., 2017; Magnin-Robert et al., 2017; Goufo et al., 2021). These studies aim to unravel physiological changes in infected vines and to understand the establishment of leaf symptoms. Few studies focus on local responses in the wood (Massonnet et al., 2017; Labois et al., 2020; Galarneau et al., 2021).

No -omics approach has been addressed to explore the molecular mechanisms in the trunk induced upon *P. chlamydospora* and *P. minimum* inoculation yet. Here, we performed a global transcriptomic and metabolomic analysis on wood samples infected either with *P. minimum*

or *P. chlamydospora*. By characterizing the grapevine trunk response to each fungus, the aim of this study was to better understand the early mechanisms underlying specific trunk responses and to determine whether the plant defense responses differ depending on the infecting pathogen.

## Materials and methods

### Biological material

#### Plants and fungi

Canes of *Vitis vinifera* cv. Cabernet Sauvignon clone 15 (Daydé Nurseries, Montans, France) were divided into two-dormant nodes cuttings. Cuttings were immediately disinfected in a bath of bleach 0.05% (2.6% active chloride) for 30 s, then rinsed twice with clear water. Then, they rested 12 h in a batch of 0.05 % 8-hydroxyquinoline sulfate (Beltanol®, Syngenta) in a cold chamber (4°C). They were then rinsed three times and planted in autoclaved (121°C, 15 min) moistened mineral wool. Three weeks after the first bud opening, they were transferred to individual pots with potting substrate (PAM2, PROVEEN Substrates) and they were kept in plant growth tents (photoperiod 12/12, 45 % humidity, 25°C).

*P. minimum* CBS 100398 and *P. chlamydospora* CBS 239.74 (Westerdijk Fungal Biodiversity Institute, Utrecht, Netherlands) were grown in Malt Extract-Agar (MEA) medium at 26°C in the dark for 6 weeks before plant inoculation.

#### Plant inoculation

Plants were produced in two times: 100 plants for transcriptomics analysis and 132 plants for metabolomics analysis. Plants were first pierced at the internode space with a drill. A plug of colonized agar with the fungal mycelium of *P. minimum* (IPm) or *P. chlamydospora* (IPch) was placed in the hole and the injury was covered with Parafilm. A set of plants were reserved as

not-injured and not-inoculated (NINi) control. Another set of plants was injured but not-inoculated (INi) as additional control. Wood sections of 2 cm long were cut around the injection point. For transcriptomics, wood samples were taken 48 hours post-inoculation (hpi), and samples were randomly pooled in four Falcon tubes ( $n = 4 \times 4$  plants/treatment). For metabolomics, wood samples were collected 3 weeks post-inoculation (wpi) and samples were also randomly pooled ( $n = 6 \times 4$  plants/treatment). In both cases, an additional set of wood samples ( $n = 9$  plants/treatment) was collected 6 wpi for fungal colonization assessment. Samples were frozen in liquid nitrogen immediately after collection and kept at  $-80^{\circ}\text{C}$  before use. Wood samples were lyophilized and ground before RNA extraction.

#### Fungal detection

Based on previous work, we considered that 6 wpi was the optimum time for ensuring fungal detection (Pouzoulet et al., 2013; Pierron et al., 2015b, 2016). Fungal colonization was evaluated via qPCR fungal DNA quantification, as described in Romeo-Oliván et al. (2021). One milliliter of DNA extraction buffer (CTAB 2%, PVPP 2%, Tris base 100 mM, EDTA 20 mM, NaCl 1.4 M, pH 8.0, 5  $\mu\text{L}$   $\beta$ -mercaptoethanol, 5  $\mu\text{L}$  RNase A) was added to 100 mg of wood powder and the mixture was incubated for 1 h at  $65^{\circ}\text{C}$ . Half a volume of a chloroform-isoamyl alcohol solution (24:1) was added next. The mixtures were incubated on ice for 5 min, then centrifuged (10 000 rpm, 15 min,  $4^{\circ}\text{C}$ ), and the supernatant was mixed with AP2 buffer from the DNeasy plant mini kit (Qiagen, USA). From this point, the extraction was made as described in the kit protocol. The final elution volume was 50  $\mu\text{L}$ . Samples were stored at  $-20^{\circ}\text{C}$ . DNA quantifications used specie-specific primers (Table 1). qPCR reactions were carried out using the GoTaq<sup>®</sup> RT-PCR systems (Promega, USA) in a final volume of 10  $\mu\text{L}$ , primers were used at a final concentration of 0.5  $\mu\text{M}$ . The qPCR reaction was conducted with an ABI 7500 Real-Time

PCR cycler (Applied Biosystems, Foster City, USA). The cycling program consisted of an initial denaturation step at 95 °C for 15 min; 40 cycles of 15 s at 95 °C (denaturation) followed by 45 s at 62 °C (annealing and extension); and an additional melting analysis of 40 min from 60 to 95 °C. The ABI SDS software v.1.4 (Applied Biosystems, Foster City, USA) was used for data analysis. Serial dilutions from  $10^5$  to  $10^2$  copies of gene, prepared as described in Pouzoulet et al. (2013), were used to create the standard curve to perform DNA quantification.

### **Transcriptomic Analysis**

#### **RNA sequencing**

First, 100 mg of wood powder were incubated in 1 mL of RNA extraction buffer (CTAB 2%, PVPP 2%, Tris 300 mM, EDTA 25 mM, NaCl 2 M, pH 8, 2 %  $\beta$ -mercaptoethanol) at 65°C for 10 minutes in continuous agitation (9 000 rpm). Samples were centrifuged (15 mins, 10 000 rpm, 4°C) and the supernatant was washed twice with one volume of Chloroform: Isoamyl alcohol (24:1, v/v) solution. After that, a mixture of 0.6 volumes of isopropanol and 0.1 volumes of  $\text{CH}_3\text{COONa}$  3M was added and samples were stored at -80°C overnight. Samples were then centrifuged (30 mins, 10 000 rpm, 4°C) and the pellet was then redissolved in 300  $\mu\text{L}$  of SSTE Buffer (NaCl 1 M, SDS 0.5 %, Tris 10 mM, EDTA 1 mM, pH 7) and 600  $\mu\text{L}$  of ethanol. The mix was transferred to the mini spin column of the RNeasy mini kit (Qiagen, USA) and the next steps were performed as indicated in the kit protocol. The RNA was eluted in 30  $\mu\text{L}$  of RNase-free water and divided in 6  $\mu\text{L}$  aliquots. DNase reactions were performed with the RQ1 RNase-Free DNase kit (Promega, USA).

RNA samples were sent to the GeT-Plage genomic platform (GenoToul, Toulouse, France) for cDNA library preparation and RNA sequencing. Each sample contained 50  $\mu\text{g}$  of RNA. Sample quality was checked before and after cDNA library preparation. The RNA Integrity Number

(RIN) threshold was set at 7, meaning that RIN from samples used in this study were no lower than 7. The TruSeq Stranded mRNA technology (Illumina, CA, USA) technology was used for cDNA library preparation. RNA sequencing was performed on an Illumina HiSeq 3000 sequenced as paired-ended reads of 150 bp. The sequencing coverage level was in average of 5.4-fold.

Fastqc (v0.11.9; Andrews, 2010) was used for control quality of raw sequencing data. Quality trimming was performed, if necessary, with sickle-trim (v1.33; Joshi and Fass, 2011) or cutadapt (v2.10; Martin, 2011) for Illumina adapters removal. Alignment was carried out with STAR (v2.7.5a; Dobin et al., 2013), using the 12X version of the *Vitis vinifera* reference genome (12X.0 version, cv PN40024)(Canaguier et al., 2017). FeatureCounts (subread v2.0.1; samtools v1.9; Liao et al., 2014) was used to extract mapped gene counts using the reference transcriptome (*Vitis\_vinifera.12X.48.chr.gtf.gz*, from Ensembl plant genomes), which allowed the estimation of the number of reads associated with each transcript. The R package SARTools (<https://github.com/PF2-pasteur-fr/SARTools>) was used to perform differential expression analysis, where all conditions were subjected to the NINi control, and thus extract differentially expressed genes (DEGs,  $p$ -value < 0.05). Gene function was annotated based on the VitisNet functional annotation database (Grimplet et al., 2009) and functional enrichment was assessed using the Fisher's exact test. A weighted gene co-expression network analysis (WGCNA) was performed in R (WGCNA package, Langfelder and Horvath, 2008) to identify modules of co-regulated genes, differently expressed among the conditions. The default value of soft-thresholding was set to 12, which fits the scale-free model with an R2 index of 0.65, approximately and the minimum module size was set to 150.

### **Metabolomic Analysis**

### Standards

Standard solutions were prepared at 100 µg/mL with natural product (NP) compounds from Chemfaces (Wuhan, Hubei) and Metasci (Metasci, Toronto, Canada).

### Wood Metabolite Extraction

Wood metabolites were extracted as described in Chervin *et al.* (2022). Briefly, 100 mg of wood powder were extracted with 1 mL of 70% EtOH with homogenization in a FastPrep by applying three cycles of 20 s at 6 m/s. Samples were kept on ice between each cycle. Then, samples were centrifuged (10 mins, 12 000 rpm, 4 °C) and supernatant was collected. The residue was retrieved, and a second extraction was performed. Finally, the two supernatants were pooled and stored at -20 °C before analysis. To assess extraction and analytical validations, an extraction blank (without plant material) and quality control (QC) samples were prepared.

### Fungal Extraction

One milliliter of ethyl acetate was added to 300 mg of agar colonized by *P. chlamydospora* or *P. minimum*. After 10 mins of sonication at room temperature, tubes were centrifuged (3 mins, 14 000 rpm, 5 °C). Finally, 800 µL of supernatant were evaporated in SpeedVac at 50 mbars and 35 °C. Dry extracts were taken up in 100 µL of ETOH 70% and transferred in LC-MS vials.

### UHPLC-HRMS profiling

A Q Exactive Plus quadrupole (Orbitrap) mass spectrometer, equipped with a heated electrospray probe (HESI II) and coupled to a U-HPLC Ultimate 3000 RSLC system (Thermo Fisher Scientific, Hemel Hempstead, U.K.) was used for conducting Ultra-High-Performance Liquid Chromatography–High-Resolution Mass Spectrometry (UHPLC–HRMS) analyses. Separations were conducted on a Luna Omega Polar C18 column (150 mm × 2.1 mm i.d., 1.6

$\mu\text{m}$ , Phenomenex, Sartrouville, France) equipped with a guard column. The mobile phase A (MPA) consisted in an aqueous solution of 0.05% formic acid (FA). The mobile phase B (MPB) consisted in an acetonitrile solution with 0.05% FA. The solvent gradient was set as follow: 100% MPA (0 - 1 min), 100% MPA to 100% MPB (1 - 22 min), 100% MPB (22 - 25 min), 100% MPB to 100% MPA (25 - 25.5 min), 100% MPA (25.5 – 28 min). The flow rate was set to 0.3 mL/min, the autosampler temperature was 5 °C, the column temperature was 40 °C, and injection volume was 5  $\mu\text{L}$ . Mass detection was performed in positive ionization (PI) mode (MS1 resolution power = 35 000 [full width at half-maximum (fwhm) at 400 m/z]; MS2 resolution power = 17 500; MS1 automatic gain control (AGC) target for full scan =  $1 \times 10^6$ ;  $1 \times 10^5$  for MS2). Ionization spray was set to a 3.5 kV voltage, and the capillary temperature was 256 °C. The mass scanning range was m/z 100–1500. Data-dependent acquisition of MS/MS spectra for the six most intense ions followed each full scan. Stepped normalized collision energy of 20, 40, and 60 eV was used for data acquisition.

### Data Processing

MS-DIAL version 4.80 (Tugawa et al., 2015) was used for UHPLC-HRMS raw data analysis. Mass feature extraction ranged between 100 and 1500 Da and 0.5 to 18.5 min. MS1 and MS2 tolerance in centroid mode were set to 0.01 and 0.05 Da, respectively. Optimized detection threshold was set to  $1 \times 10^5$  and 10 for MS1 and MS2, respectively. Peaks were aligned to a quality control (QC) reference file, with a retention time tolerance of 0.15 min and a mass tolerance of 0.015 Da. An in-house database built on MS-FINDER model (Tugawa et al., 2016) allowed peak annotation.

MS-CleanR workflow version 1.0 (Fraisier-Vannier et al., 2020) was employed for cleaning MS-DIAL resulting data. A minimum blank ratio of 0.8, a maximum relative standard deviation

(RSD) of 40, and a relative mass defect (RMD) ranging from 50 to 3 000 were set for all filters selected. For feature relationships detection, the maximum mass difference was set to 0.005 Da, and the maximum RT difference to 0.025 min. The Pearson correlation links were considered with correlation  $\geq 0.8$  and statistically significant with  $\alpha = 0.05$ . The most intense and the most connected peaks were kept in each cluster.

Feature annotations were carried out with MS-FINDER version 3.52. The MS1 and MS2 tolerances were respectively set to 5 and 10 ppm. Formula finder were only processed with C, H, O, N, P, and S atoms. The *Vitis* (genus), *Vitaceae* (family) and *Togniniaceae* (the family of the two pathogenic fungi) databases (DBs) were constituted with the dictionary of natural product (DNP, CRC press, DNP on DVD v. 28.2). Within the generic DBs from MS-FINDER we selected KNApSAcK, PlantCyc, NANPDB, UNPD and COCONUT. Annotation prioritization was done by ranking *Vitis* DB, followed by *Vitaceae* DB, *Togniniaceae* DBs and finally generic DBs, using the final MS-CleanR step.

#### Mass Spectral Similarity Network

MetGem version 1.2.2 was used to create mass spectral similarity networks was created (cosine score cut off = 0.7) with a maximum of ten connections between nodes. The resulting networks were transferred into Cytoscape12 version 3.9.1 interface. Nodes were differently colored depending on the chemical classes and the size of highlighted markers was increased. To tune markers representative distribution in each treatment, OPLS-DA coefficient values were used to modulate node size. High values were correlated to characteristic features of the studied class. Node size was modified depending on these coefficient values.

#### Statistical Analysis

Statistical analyses were performed with Simca v 14.1. All data were UV-(unit variance) scaled before multivariate analysis. Principal component analysis (PCA) and orthogonal projection to latent structures discriminant analysis (OPLS-DA) were performed. The validity of models was assessed using CV-anova (p-value < 0.05).

T-test (p < 0.05) based on unpaired experimental design were used to check markers significance with GraphPad Prism 8 version 8.3.0 (San Diego, California). Heatmap of revealed markers based on average peak area was built with the web-interface MetaboAnalyst version 4.0 (Chong et al., 2019).

## Results

### Transcriptomics analysis

Successful fungal colonization was assessed via qPCR quantifications to confirm the infection. The results showed that both fungi were able to colonize the trunk 6 wpi (Fig. 1). Transcriptomics analysis was performed on healthy or infected wood tissue 48 hpi. We performed a differential expression analysis on transcript normalized counts, comparing all the conditions to the Not-Injured and Not-infected (NINi) control. The comparison between Injured and Not infected (INi) vs NINi, (p-value < 0.05 and logFC = |1|) identified a total of 501 differentially expressed genes (DEGs; 61 downregulated, 440 upregulated). On the other hand, the pathogens triggered modifications on the expression of 4073 genes (1968 downregulated, 2105 upregulated), in the case of *P. minimum*, and 2224 genes (1014 downregulated, 1210 upregulated), for *P. chlamydospora*. From these, we found that 422 and 258 DEG, for *P. minimum* and *P. chlamydospora*, respectively, were shared with the injury (Fig. 2A). These DEGs were thus discarded for the rest of the analysis in the aim of keeping only the genes whose expression was modified uniquely upon pathogen infection. We compared then

those DEGs specifically up- or down- regulated in the wood upon infection to determine which were specific to each pathogen or common to both (Fig. 2B). After the infection with *P. minimum*, 994 genes were found to be upregulated and 1237 genes were downregulated. *P. minimum* was found to modify the expression of a larger total set of DEGs than *P. chlamydospora* (2231 DEGs vs 546 DEGs). Nevertheless, we found that 1661 DEGs were regulated by both pathogens, which represented 45.5 % of the DEGs regulated by *P. minimum* and 84.5 % of those regulated by *P. chlamydospora*. This very first global result already indicates a specific trunk response which depends on the infecting pathogen.

### **Functional main differences between the transcriptomic response induced by the two pathogens.**

To highlight main differences, a global functional enrichment analysis was performed on the DEGs specifically regulated by *P. minimum* or *P. chlamydospora* (Fig. 2C, Supplementary Table S2). For both pathogens, we observed that the shared enriched functional categories were Protein Kinase Signaling, Transcription factors, Biotic Stress Response, Protein metabolism and Electrochemical Potential-driven Transporters categories. Main significant differences were found among DEGs associated with Secondary metabolism, especially for Phenylpropanoid biosynthesis with 32 DEGs for *P. minimum* and only 8 DEGs for *P. chlamydospora*. There were also differences associated with Hormone signaling, Signaling and Transport categories. Differences were also found in DEGs associated with Thiamine biosynthesis and Riboflavine biosynthesis (respectively down- and up-regulated by *P. chlamydospora*), Organic acid metabolism or Cytoskeleton organization and biogenesis (up-regulated by *P. minimum*).

### **Gene expression analysis**

The total 4438 DEGs modified by both pathogens were divided in nine modules of co-expressed genes through a Weighted Gene Co-expression Network Analysis (WGCNA). A gene tree based on pairwise correlation was constructed and, from this dendrogram, modules of coregulated genes were extracted. One unique color was associated with each module as identifying label (Fig. 3A). Each module corresponds to a group of coregulated genes that forms biological networks built from gene expression data. The hierarchical distance between modules was calculated and represented as a module dendrogram to illustrate the relationship between modules (Fig. 3B). The eigengenes from each module, which represent the principal component of the variability in the module, were calculated to gain further insight on the average gene expression of the module in each condition (Fig. 3C). According to this analysis, brown and red modules were up-regulated in the presence of *P. minimum*, while grey and pink modules were upregulated in the presence of *P. chlamyospora*.

A functional enrichment analysis was performed now for each module. Phenylpropanoid biosynthesis, Ethylene-mediated signaling pathways and Auxin-mediated signaling pathways were some of the main enriched functions in the brown and red module. ABA-mediated signaling pathways, Jasmonate-mediated signaling pathways and Plant-pathogen interaction were also enriched in the red module. Concerning the pink and grey module, among the enriched functions we found G-protein signaling, Protein phosphatase PP2C, Auxin inactivation, ABA biosynthesis and ABA-mediated signaling pathways. The blue, green and yellow modules were analyzed together, as they presented a similar expression pattern. The same was done for the black and turquoise module. Functions associated with the primary metabolism, such as Nucleic acid metabolism and Protein metabolism were enriched among the genes belonging to the blue-green-yellow modules. Concerning hormone signaling, the functions enriched in the blue-green-yellow modules were Auxin transport, ABA-mediated

signaling pathways, Cytokinin-mediated signaling. For secondary metabolism, we found Flavonoid biosynthesis and Diterpenoid metabolism enriched in these three modules. Protein kinase signaling, Plant-pathogen interaction, Glycerophospholipid metabolism, Phenylpropanoid metabolism and Monoterpenoid metabolism are some of the enriched functions in the black-turquoise modules. Therefore, genes associated with these functional categories are up-regulated by both pathogens.

We extracted the genes contained in each module and we conducted a gene expression pattern analysis on each module individually. The aim of this analysis was to determine if there were differences between the responses to *P. minimum* and *P. chlamydospora* inside the modules. The analysis allowed the extraction of several clusters of genes that were differentially expressed by *P. minimum* or *P. chlamydospora* (Fig. 3D). For instance, cluster 3 in the black-turquoise module, cluster 3 in the blue-green-yellow module, cluster 1 in the red module and cluster 1 in the brown module are specifically up-regulated by *P. minimum*. On the other hand, clusters 5 and 8 on the black-turquoise module, cluster 4 in the blue-green-yellow module and cluster 3 in the brown module were up-regulated by *P. chlamydospora*. Gene functions on these cluster showed dissimilarities between the gene signatures associated with each pathogen. For instance, *P. minimum* seem to enhance the expression of genes associated with Phenylpropanoid biosynthesis (Red module, p-value 2.09E-05; brown module, p-value 6.45E-04) and Terpenoid biosynthesis (Blue-green-yellow module, cluster 3, p-value 1.21E-02), whereas Flavonoid biosynthesis (Blue-green-yellow module, cluster 4, p-value 5.00E-02) appears to be up-regulated in response to *P. chlamydospora*. We found many genes associated with Biotic stress response in these clusters: 11 genes in cluster 3 (blue-green-yellow module), 6 genes in cluster 1 (red module) and 9 genes in cluster 1 (brown) up-regulated specifically by *P. minimum*. In cluster 5 (black-turquoise module), 10 genes were

associated with Biotic stress, from which 7 code for putative R-proteins. We also found that clusters 4 in the black-turquoise module and cluster 2 in the blue-green-yellow module were down-regulated by *P. minimum* and *P. chlamydospora*, respectively.

The functional analysis of all those clusters also provided hints for the understanding of the underlying mechanisms responsible for this different primary response. Among the DEGs grouped in those clusters, we found several genes coding for putative NBS-LRR proteins (VIT\_16s0050g00250, VIT\_03s0038g01760, VIT\_13s0156g00540 and VIT\_11s0052g00390 for *P. minimum*; VIT\_11s0118g00080, VIT\_10s0042g00450, VIT\_03s0017g00610 and VIT\_19s0014g00570 for *P. chlamydospora*). These proteins are known to be involved in pathogen recognition and, therefore, they have an important role in the first steps of the induction of the plant defense (McHale et al., 2006; Cesari, 2018). Each fungus appears to induce the expression of specific NBS-LRR, which may trigger different down-stream signaling pathways. DEGs related to Signaling pathways regulated by *P. minimum* seem to be linked to Calcium sensors and signaling and many genes coding for putative protein kinases are also up-regulated. On the contrary, none of the DEGs in the cluster regulated by *P. chlamydospora* were associated with Calcium sensors and signaling, but several putative mitogen-activated protein kinases (MAPK) were upregulated in these clusters. Hormone signaling was also found different depending on the pathogen. *P. minimum* modifies the expression of a great number of genes associated with hormone signaling. While *P. chlamydospora* seem to affect specially auxin and cytokinin metabolism, *P. minimum* seem to interfere with ethylene-, auxin-, abscisic acid (ABA)- and jasmonic acid (JA)-mediated signaling.

### **Deciphering characteristic biochemical markers on infected wood**

UHPLC-HRMS profiles of all the extracts (3 weeks after inoculation) afforded 472 features ( $m/z$ -RT pairs) in PI mode after application of the MS-CleanR workflow. PCA was performed to provide an unsupervised overview of the LC-MS fingerprints (Fig. 4). The two first principal components explained 41.2% of the total variance. QC samples were centered on the PCA plot, demonstrating the high reproducibility of the analysis. IPch samples were separated by PC1 whereas INi and IPm samples were mainly separated by PC2.

To discriminate metabolites from *Vitis* wood to metabolites coming from the studied fungi, comparison of chromatographic profiles of fungal cultures and wood samples was done and conducted to 19 common features, based on  $m/z$  and MS/MS fragmentation (dot and reverse dot product > 750). On these 19 features, only two were annotated with fungal *Togniaceae* DB, while all others were annotated with generic DBs (supplementary Table S3). Thus, most detected metabolites appeared to be plant metabolites. Interestingly, by comparing the distribution of all metabolites among experimental conditions through a heatmap (Fig. S1), samples inoculated with one of the fungi were clustered together meaning that fungi inoculation seem to change in a similar way the wood metabolome, compared to the injury. The major significant discriminant features involved in specific plant responses to *P. chlamydospora*, and *P. minimum* were selected with the use of a supervised data mining approach. Two OPLS-DA models were built to compare infested wood to control samples (IPch vs INi and IPm vs INi). In order to assess the contribution of the detected metabolites to *P. chlamydospora* or *P. minimum* inoculation, the correlation vectors  $\text{corr}(tp, X)$ , computed from the loadings of the predictive component (first latent variable) of both models were combined to build a shared and unique structure plot (SUS-plot). This representation (Wiklund et al., 2008) allowed highlighting features related to the specific metabolomic responses to each fungus according to their position (Fig. 5). In this representation, characteristic compounds

detected in higher abundance in IPch samples were displayed in the upper left square (blue triangle); those in higher abundance in IPm samples in the lower-right square (yellow triangle) and the ones in higher abundance in INi samples in the lower-left square (black triangle). The upper-right square displayed common features to IPch and IPm (purple triangle).

Based on this SUS-plot, extreme metabolites in each square corresponding to the more representative features were thus selected and according to t-test values ( $p$ -value < 0.05), the topmost significant metabolites were retained (Fig. 6). Thus, five significant metabolites were detected in higher abundance in IPch samples (compounds 7, 9, 24, 25 and 26), ten in IPm samples (compounds 4, 5, 6, 15, 20, 21, 22, 23, 27 and 29), five in INi samples (compounds 1, 8, 13, 16 and 31) as well as eleven shared compounds between IPch and IPm (compounds 2, 3, 10, 11, 12, 14, 17, 18, 19, 28 and 30). Putative annotations of these 31 significant markers are displayed in Table 2. Feature annotations were obtained by interrogating simultaneously *Vitis*, *Vitaceae*, *Togniniaceae* and generic databases of natural products in MS-FINDER. Only annotations with a MS-FINDER score above 6, correlated to strong chemical class hypothesis, were retained.

Trans-resveratrol [3] and pinostilbene [5] displayed an identification of level 1 according to the Metabolomics Standards Initiative (MSI) (Sumner et al., 2007) as their MS/MS fragments and retention time match with standards injected in the same analytical conditions (RT similarity score > 850 ; similarity spectrum score > 800). Seventeen compounds displayed an identification of level 2, as putative structures based on *in silico* MS/MS comparison with DBs were proposed. Among them, two main chemical classes were highlighted: flavonoids and stilbenes. The molecular formulae of these compounds matched structures already identified in *Vitis* genus, except the flavonoid [21] annotated with generic DBs. Compounds [1], [7] and [14] were respectively annotated as indole, amine and glycerophospholipid classes. Finally,

twelve compounds obtained an annotation score with MS-FINDER under 6. Therefore, only molecular formulas were retained, displaying an identification of level 4.

To help interpreting chemical classes of these unknown compounds and better observe the distribution of detected features in each experimental condition, a mass spectral similarity network was built (Fig. 7A) and OPLS-DA coefficients were used to modulate network node size. These coefficients represent the close correlation between a feature and a treatment condition thus high values correspond to characteristic features of a given class. In the network visualization, biggest nodes correspond to highest OPLS-DA coefficients, whereas smallest nodes correspond to smallest coefficient values (for INi: Fig. 7B, for IPch: Fig. 7C and IPm: Fig. 7D). Modulating node size allowed the highlight of features of interest which were more precisely studied. Mainly, two stilbene clusters and two flavonoid clusters seem to stand out, respectively corresponding to clusters 1 - 4, and clusters 2 – 3 (Fig. 7). Stilbene clusters 1 and 4 were well-represented in all conditions, as several nodes were similarly highlighted in Fig. 7B (INi), C (IPch) and D (IPm). However, distinct compounds were also revealed as materialized by specific emphasized nodes for one specific treatment. Similarly, flavonoids of cluster 3 were quite equally represented in IPch and IPm networks but less marked in INi samples (Fig. 7 C-D). Common and distinct compounds were revealed. On the contrary, flavonoids of cluster 2 were more represented in IPm than IPch or INi samples (Fig. 6D). Separation of flavonoid clusters 2 and 3 (Fig 7 C-D) in two independent groups suggests the presence of specific flavonoid structures overproduced in presence of *P. minimum*. The difference on the elution time between clusters 2 and 3 suggest that compounds of cluster 2 were more lipophilic than those of cluster 3, as they were eluted at higher retention times.

Based on this mass spectral similarity network, it was possible to attribute putative chemical classes to the unknown compounds. Thus, compounds [6], [15], [20], [22] and [23] were

tagged as flavonoid derivative and compound [13] as a stilbene derivative since they belong to corresponding clusters.

Besides, several putative markers presented the same  $m/z$  and MS/MS pattern with different retention times and should be isomeric derivatives. Thus, compounds [24], [25] and [26] were annotated as Diptoindonesin B derivatives as the same annotation was obtained with MS-FINDER. Similarly, compounds [17] and [18] were annotated as procyanidin A1 derivatives. Compound [21] was annotated as an 8-O-methylated flavonoid. As annotation for compound [20], displaying a similar  $m/z$  as [21], was not sufficient in term of scoring, it remained as unknown. Compounds [22] and [23] displayed low annotation score thus both remained as unknown compounds. In this context, several compounds were already highlighted in the pathosystem *P. chlamydospora* in combination with *P. minimum* (Chervin et al., 2022): the stilbenoid [12], the glycerosphospholipid [14] and the flavonoids [18] and [19]. Fungal metabolomes were also processed to well separate metabolites from *Vitis* wood to metabolites coming from the studied fungi. Interestingly, three of defined markers were found in common. The indoline [1] was found in the metabolome profile of *P. chlamydospora* while the benzoic acid [4] and the LysoPC [14] were found in the metabolome profile of *P. minimum*.

Therefore, flavonoid derivatives were mainly found as compounds overproduced during the infection with *P. chlamydospora* or *P. minimum* and appeared to be specific markers of wood infestation. Nevertheless, several unknown more lipophilic flavonoids were specially produced in presence of *P. minimum*. Stilbenes derivatives were found in all experimental conditions, but Diptoindonesin B derivatives were particularly overproduced in presence of *P. chlamydospora*.

## Discussion

Defense responses in woody tissues have been considered historically as generalist responses, as described by the CODIT (Compartmentalization Of Decay In Trees) model (Shigo and Marx, 1977). This model postulates that, regardless of the nature of the attack, the wood will respond with the formation of different physical barriers in the aim to prevent the propagation of the decay. However, in the case of grapevine trunk diseases, several pieces of evidence suggest that defense responses in the trunk differ depending on the attacking pathogen.

Here, we aimed to characterize the specific grapevine wood early responses to *P. chlamydospora* and *P. minimum*. Transcriptomic reprogramming analysis at this point gave insight into the different molecular mechanisms activated upon perception of either *P. minimum* or *P. chlamydospora*. At this timepoint, the first contact has been made between the wood and the pathogens, but the fungi have not colonized yet the wood (Pierron et al., 2015a). Metabolomics analysis at this 3 wpi show the results of these first responses in the infection point. At this timepoint, the pathogens have not reached the vascular internal system but have colonized the infection point (Pierron et al., 2015a). In both analyses, we found significant differences between biological conditions, showing that both pathogens are perceived differently and that plant responses also differ depending on the pathogen. The analysis of transcriptomic reprogramming of wood gene expression upon *P. chlamydospora* and *P. minimum* infection revealed a clear difference on the number of genes differentially expressed in response to each fungus. The totality of the DEGs were first separated into networks of co-regulated genes and these into clusters based on the gene expression pattern. These analyses allowed the identification of several groups of genes specifically regulated by either *P. minimum* or *P. chlamydospora* and functional analysis on these modules showed biological differences.

Among functional differences, we found several putative NBS-LRR and R proteins encoding genes differently expressed in response to either *P. chlamydospora* or *P. minimum*, suggesting that each fungus is specifically perceived. The family of Nucleotide-Binding Site Leucine-Rich Repeat (NBS-LRR) proteins are the major class of resistance proteins (R proteins) and have an important role on pathogen effector recognition and disease resistance (Cesari, 2018). The recognition of the aggressor triggers a plethora of signaling events, that in turn activate downstream defense-related genes (Jones and Dangl, 2006). Down-stream signaling after microbe detection includes different mechanisms including calcium signaling, protein phosphorylation/dephosphorylation and mitogen-activated protein kinase (MAPK) protein signaling (Jones and Dangl, 2006). Concerning functional enriched categories, Calcium sensors and signal and Protein kinase signaling, from which we found several C2 domain-containing protein kinases, were differently regulated in response to *P. minimum*. In the case of *P. chlamydospora*, the infection up-regulates several genes coding for putative MAPK proteins. These differences suggest that each fungus trigger different signaling mechanisms, which support the hypothesis that they may also exist different perception mechanisms for *P. minimum* and *P. chlamydospora*.

Hormone signaling is also a key component of signal transduction in plant defense responses. Phytohormones are small metabolites acting as secondary messengers involved in a wide range of plant physiological processes (Pieterse et al., 2012) and they have critical roles in plant defense (Vallad and Goodman, 2004; Liu et al., 2016). Transcriptomic analysis highlighted a different reprogramming on the expression of genes involved in hormonal signaling depending on the infecting pathogen. For instance, ABA- and ethylene signaling-related genes were enriched among DEGs in response to each fungus individually. This over-expression was also observed during the combined infection with both pathogens, as we

showed in a previous study (Romeo-Oliván et al., 2022). The phytohormone ABA is known to be involved mainly in abiotic stress response, especially in drought stress response, but it is reported to also have roles in plant development and biotic stress response (Mauch-Mani and Mauch, 2005; Robert-Seilaniantz et al., 2011; Yoshida et al., 2019; Chen et al., 2020). In some cases, ABA was found to play a negative role on disease resistance (Mauch-Mani and Mauch, 2005; Ton et al., 2009). In grapevine berries, exposure to exogenous ABA decreases the expression of defense response-related genes in response to *Botrytis cinerea* (Hatmi et al., 2018). Therefore, ABA could be a mark of pathogen susceptibility rather than a defense response. Ethylene-mediated responses are known to play a critical role in plant defense (Bari and Jones, 2009). Ethylene is known to orchestrate different plant responses, especially plant defense responses against necrotic pathogens. In grapevine, it has been associated to xylem occlusion in response to *Xylella fastidiosa*, the causal bacterium of grapevine Pierce's disease (Pérez-Donoso et al., 2007). In addition, Ingel et al. (2021) showed a correlation between ethylene signaling gene reprogramming upon *X. fastidiosa* infection and tylose formation. Xylem occlusion is a classic symptom of esca disease. Thus, ethylene might play a key role in the coordination of the trunk's cellular responses in response to esca associated pathogens. Fungal attack is an important biotic stress and plant defense response can also involve specific metabolites, such as polyphenols and phenylpropanoids (Tuladhar et al., 2021). A great number of genes associated to Phenylpropanoid metabolism and synthesis undergo an expression reprogramming in response to each fungus. Metabolomics analysis revealed two main significant chemical classes of metabolites over-produced in the wood upon infection: flavonoids and stilbenes. These two chemical classes are known as phytoalexins since they play a role in plant defense, as in pathogen attack (Samanta et al., 2011; Ahuja et al., 2012). Previous studies on metabolic response of grapevine to pathogen infection highlighted the

positive correlation between flavonoids and stilbenes production with infection (Labois et al., 2020; Galarneau et al., 2021; Chervin et al., 2022). Most annotated markers were found in *Vitis* database. Interestingly, three of them were also found in fungal metabolome but seem to be ubiquitous as they were not specifically annotated with fungal genus database.

Stilbenes are found as constitutive compounds of *Vitaceae* (Goufo et al., 2019, 2021). It could then easily explain their presence in all studied matrices. They were largely represented in inoculated samples. Mainly stilbene oligomers were observed, and they were previously reported as more toxic than resveratrol monomers (Lambert et al., 2012; Gabaston et al., 2017). Some stilbenoid compounds were equally expressed in presence of *P. minimum* or *P. chlamydospora*, in comparison to control samples, such as trans-resveratrol, but specific responses were also highlighted. Three Diptoindonesin B derivatives were revealed more specific to *P. chlamydospora* infection whereas pinostilbene, a resveratrol derivative, was slightly more abundant in response to *P. minimum* infection.

Flavonoids, which were also mainly found in inoculated samples, are present in many plants and are often overproduced in stress conditions (Shah and Smith, 2020). This study revealed that some flavonoids, such as the procyanidin derivatives, were equally overproduced upon inoculation with *P. minimum* and *P. chlamydospora* in comparison to control samples, whereas others were more induced by than by *P. minimum*. Interestingly, in the mass spectral similarity network, these two flavonoid groups were separated in two distinct clusters. As this network is based on MS/MS fragmentation similarity linked to similarity of structures, it appeared that specific lipophilic flavonoids seem correlated to *P. minimum* infection. Unfortunately, based on lack of mass spectral information on these features, no structure elucidation could be done, and further analysis should be requested to suggest potential annotations.

We observed an unequal colonization 6 wpi when fungi were inoculated separately. Given the fact that only one timepoint was considered in our study, this observation might lead to the hypothesis that these metabolic differences could be also related to a different temporality on the infection process of each fungus. If one of the fungi were more performant in terms of colonization, it may trigger defense responses faster than the other, creating a temporal gap. However, this uneven colonization was not observed when both fungi were co-inoculated (Chervin et al., 2022). Thus, another hypothesis could be that specific molecular defense responses in the wood against *P. chlamydospora* limit or slow down its growth when it infects the wood alone. In addition, some of the compounds highlighted in our metabolomic analysis, such as resveratrol ([3], [24], [25] and [26]), have shown effective antifungal properties *in vitro* conditions against *P. chlamydospora* (Chervin et al., 2022). Unfortunately, little is known about the colonization process of *P. minimum* and *P. chlamydospora*, nor about the effect of this compounds in the development of *P. minimum*. Further research is necessary to elucidate this question.

The combination of transcriptomic and metabolomic analyses were conducted in parallel to propose an overall view of wood biochemistry after infection with two main grapevine pathogens, *P. chlamydospora* and *P. minimum*. The objective was to study the specific local defense response against these pathogens. Transcriptomics revealed various genes differentially expressed. They particularly concern signal functions such as calcium or hormonal signaling as well as primary and secondary metabolite expressions, which were over up-regulated in presence of *P. minimum*. Thirty-one putative markers were revealed through the UHPLC-HRMS based metabolomic analysis and were mainly annotated as flavonoids and stilbenes, which are known to be involved in plant defense. Several were commonly elicited by *P. minimum* or *P. chlamydospora* but interestingly, one cluster of more lipophilic flavonoids

seem more specific to the response to *P. minimum*. Altogether, in this study, both transcriptomic and metabolomic results show that grapevine woody tissues can differentially respond to *P. minimum* and *P. chlamydospora* and suggest that they may exist specific perception mechanisms associated with each fungus.

### **Acknowledgments**

MetaToul (Toulouse metabolomics & fluxomics facilities, [www.metatoul.fr](http://www.metatoul.fr)) is part of the French National Infrastructure for Metabolomics and Fluxomics MetaboHUB-ANR-11-INBS-0010. The authors are grateful to the GeT-Plage platform (GenoToul, Toulouse) for their work and the quality of the RNA sequencing.

### **Authors contribution**

GM, VPP, SF, JD, BD and AJ supervised the project. JC carried out the plant extraction, the analytical workflow and the data processing and interpretation. ARO carried out the plant culture and treatment as well as the transcriptomic analysis and interpretation. CB helped with plant culture, plant inoculation and with q RT PCR reactions. OR, VPP, GM, AJ contributed to the understanding and discussion of the results. JC and ARO authored the article. All authors have revised and have agreed the published version of the manuscript.

### **Conflict of interest**

The authors declare that the research was performed in the absence of any commercial or financial relationships that could be construed as a potential conflict of interest.

### **Data availability**

The datasets presented in this study can be found in online repositories. The names of the repositories and accession numbers can be found below: PRJNA817518 (NCBI) and 10.5281/zenodo.5779519.

### Literature cited

Ahuja, I., Kissen, R., and Bones, A. M. (2012). Phytoalexins in defense against pathogens.

*Trends Plant Sci.* 17, 73–90. doi:10.1016/J.TPLANTS.2011.11.002.

Andrews, S. (2010). Babraham Bioinformatics - FastQC A Quality Control tool for High

Throughput Sequence Data. *Soil* 5, 47–81. doi:10.1016/0038-0717(73)90093-X.

Bari, R., and Jones, J. D. G. (2009). Role of plant hormones in plant defence responses. *Plant*

*Mol. Biol.* 69, 473–488. doi:10.1007/S11103-008-9435-0.

Bertsch, C., Ramírez-Suero, M., Magnin-Robert, M., Larignon, P., Chong, J., Abou-Mansour, E.,

et al. (2013). Grapevine trunk diseases: Complex and still poorly understood. *Plant*

*Pathol.* 62, 243–265. doi:10.1111/j.1365-3059.2012.02674.x.

Blanchette, R. a, and Biggs, a R. (1992). Defense mechanisms of woody plants against fungi.

*Springer Ser. wood Sci.*, 458.

Bruez, E., Lecomte, P., Grosman, J., Doublet, B., Bertsch, C., Fontaine, F., et al. (2013).

Overview of grapevine trunk diseases in France in the 2000s. *Phytopathol. Mediterr.* 52,

262–275. doi:10.14601/Phytopathol\_Mediterr-11578.

Canaguier, A., Grimplet, J., Di Gaspero, G., Scalabrin, S., Duchêne, E., Choisne, N., et al. (2017).

A new version of the grapevine reference genome assembly (12X.v2) and of its annotation (VCost.v3). *Genomics Data* 14, 56–62. doi:10.1016/j.gdata.2017.09.002.

- Cesari, S. (2018). Multiple strategies for pathogen perception by plant immune receptors. *New Phytol.* 219, 17–24. doi:10.1111/NPH.14877.
- Chen, K., Li, G. J., Bressan, R. A., Song, C. P., Zhu, J. K., and Zhao, Y. (2020). Abscisic acid dynamics, signaling, and functions in plants. *J. Integr. Plant Biol.* 62, 25–54. doi:10.1111/JIPB.12899.
- Chervin, J., Romeo-Oliván, A., Fournier, S., Puech-Pages, V., Dumas, B., Jacques, A., et al. (2022). Modification of Early Response of *Vitis vinifera* to Pathogens Relating to Esca Disease and Biocontrol Agent Vintec® Revealed By Untargeted Metabolomics on Woody Tissues. *Front. Microbiol.* 13, 234. doi:10.3389/fmicb.2022.835463.
- Chong, J., Wishart, D. S., and Xia, J. (2019). Using MetaboAnalyst 4.0 for Comprehensive and Integrative Metabolomics Data Analysis. *Curr. Protoc. Bioinforma.* 68. doi:10.1002/CPBI.86.
- Czemmel, S., Galarneau, E. R., Travadon, R., McElrone, A. J., Cramer, G. R., and Baumgartner, K. (2015). Genes expressed in grapevine leaves reveal latent wood infection by the fungal pathogen *Neofusicoccum parvum*. *PLoS One* 10. doi:10.1371/JOURNAL.PONE.0121828.
- Dobin, A., Davis, C. A., Schlesinger, F., Drenkow, J., Zaleski, C., Jha, S., et al. (2013). STAR: ultrafast universal RNA-seq aligner. *Bioinformatics* 29, 15–21. doi:10.1093/BIOINFORMATICS/BTS635.
- Fontaine, F., Gramaje, D., Armengol, J., Smart, R., Nagy, Z. A., Borgo, M., et al. (2016). Grapevine Trunk Diseases. A review. Available at: [www.oiv.int](http://www.oiv.int).
- Fraisier-Vannier, O., Chervin, J., Cabanac, G., Puech, V., Fournier, S., Durand, V., et al. (2020).

MS-CleanR: A Feature-Filtering Workflow for Untargeted LC-MS Based Metabolomics.

*Anal. Chem.* 92, 9971–9981.

doi:10.1021/ACS.ANALCHEM.0C01594/SUPPL\_FILE/ACOC01594\_SI\_006.XLSX.

Gabaston, J., Cantos-Villar, E., Biais, B., Waffo-Teguo, P., Renouf, E., Corio-Costet, M. F., et al.

(2017). Stilbenes from *Vitis vinifera* L. Waste: A Sustainable Tool for Controlling

Plasmopara Viticola. *J. Agric. Food Chem.* 65, 2711–2718. doi:10.1021/acs.jafc.7b00241.

Galarneau, E. R. A., Lawrence, D. P., Wallis, C. M., and Baumgartner, K. (2021). A comparison

of the metabolomic response of grapevine to infection with ascomycete wood-infecting

fungi. *Physiol. Mol. Plant Pathol.* 113. doi:10.1016/J.PMPP.2020.101596.

Gimeno-Gilles, C., Lelièvre, E., Viau, L., Malik-Ghulam, M., Ricoult, C., Niebel, A., et al. (2009).

ABA-Mediated inhibition of germination is related to the inhibition of genes encoding

cell-wall biosynthetic and architecture: modifying enzymes and structural proteins in

medicago truncatula embryo axis. *Mol. Plant* 2, 108–119. doi:10.1093/mp/ssn092.

Gonçalves, M. F. M., Nunes, R. B., Tilleman, L., Van De Peer, Y., Deforce, D., Nieuwerburgh, F.

Van, et al. (2019). Dual RNA Sequencing of *Vitis vinifera* during *Lasiodiplodia theobromae*

Infection Unveils Host–Pathogen Interactions. *Int. J. Mol. Sci.* 2019, Vol. 20, Page 6083

20, 6083. doi:10.3390/IJMS20236083.

Goufo, P., Marques, A. C., and Cortez, I. (2019). Exhibition of local but not systemic induced

phenolic defenses in *vitis vinifera* L. Affected by brown wood streaking, grapevine leaf

stripe, and apoplexy (ESCA complex). *Plants* 8. doi:10.3390/plants8100412.

Goufo, P., Singh, R. K., and Cortez, I. (2021). Metabolites Differentiating Asymptomatic and

- Symptomatic Grapevine Plants (*Vitis vinifera* 'Malvasia-Fina') Infected with Esca Complex Disease-Associated Fungi. *Biol. life Sci. forum* 11, 87. doi:10.3390/iecps2021-11923.
- Gramaje, D., Aroca, Á., Raposo, R., García-Jiménez, J., and Armengol, J. (2009). Evaluation of fungicides to control Petri disease pathogens in the grapevine propagation process. *Crop Prot.* 28, 1091–1097. doi:10.1016/j.cropro.2009.05.010.
- Gramaje, D., Urbez-Torres, J. R., and Sosnowski, M. R. (2018). Managing grapevine trunk diseases with respect to etiology and epidemiology: Current strategies and future prospects. *Plant Dis.* 102, 12–39. doi:10.1094/PDIS-04-17-0512-FE.
- Grimplet, J., Cramer, G. R., Dickerson, J. A., Mathiason, K., van Hemert, J., and Fennell, A. Y. (2009). Vitisnet: "Omics" integration through grapevine molecular networks. *PLoS One* 4. doi:10.1371/journal.pone.0008365.
- Guerin-Dubrana, L., Fontaine, F., and Mugnai, L. (2019). Grapevine trunk disease in European and Mediterranean vineyards: Occurrence, distribution and associated disease-affecting cultural factors. *Phytopathol. Mediterr.* 58, 49–71. doi:10.13128/Phytopathol\_Mediterr-25153.
- Hatmi, S., Villaume, S., Trotel-Aziz, P., Barka, E. A., Clément, C., and Aziz, A. (2018). Osmotic stress and ABA affect immune response and susceptibility of grapevine berries to gray mold by priming polyamine accumulation. *Front. Plant Sci.* 9. doi:10.3389/FPLS.2018.01010/FULL.
- Ingel, B., Reyes, C., Massonnet, M., Boudreau, B., Sun, Y., Sun, Q., et al. (2021). *Xylella fastidiosa* causes transcriptional shifts that precede tylose formation and starch

depletion in xylem. *Mol. Plant Pathol.* 22, 175–188. doi:10.1111/MPP.13016.

Jones, J. D. G., and Dangl, J. L. (2006). The plant immune system. *Nature* 444, 323–329. doi:10.1038/NATURE05286.

Joshi, N. A., and Fass, J. N. (2011). Sickle: a sliding-window, adaptive, quality-based trimming tool for FastQ files.

Labois, C., Wilhelm, K., Laloue, H., Tarnus, C., Bertsch, C., Goddard, M. L., et al. (2020). Wood Metabolomic Responses of Wild and Cultivated Grapevine to Infection with *Neofusicoccum parvum*, a Trunk Disease Pathogen. *Metabolites* 10, 1–19. doi:10.3390/METABO10060232.

Lambert, C., Bisson, J., Waffo-Téguo, P., Papastamoulis, Y., Richard, T., Corio-Costet, M. F., et al. (2012). Phenolics and their antifungal role in grapevine wood decay: Focus on the Botryosphaeriaceae family. *J. Agric. Food Chem.* 60, 11859–11868. doi:10.1021/jf303290g.

Langfelder, P., and Horvath, S. (2008). WGCNA: An R package for weighted correlation network analysis. *BMC Bioinformatics* 9. doi:10.1186/1471-2105-9-559.

Larignon, R., and Dubos, B. (1997). Fungi associated with esca disease in grapevine. *Eur. J. Plant Pathol.* 103, 147–157. doi:10.1023/A:1008638409410.

Lemaitre-Guillier, C., Dufresne, C., Chartier, A., Cluzet, S., Valls, J., Jacquens, L., et al. (2021). VOCs Are Relevant Biomarkers of Elicitor-Induced Defences in Grapevine. *Molecules* 26. doi:10.3390/MOLECULES26144258.

Liao, Y., Smyth, G. K., and Shi, W. (2014). featureCounts: an efficient general purpose program

for assigning sequence reads to genomic features. *Bioinformatics* 30, 923–930. Available at: <http://subread.sourceforge.net>

Lima, M. R. M., Felgueiras, M. L., Cunha, A., Chicau, G., Ferreres, F., and Dias, A. C. P. (2017).

Differential phenolic production in leaves of *Vitis vinifera* cv. Alvarinho affected with esca disease. *Plant Physiol. Biochem.* 112, 45–52. doi:10.1016/j.plaphy.2016.12.020.

Lima, M. R. M. M., Ferreres, F., and Dias, A. C. P. P. (2012). Response of *Vitis vinifera* cell

cultures to *Phaeomoniella chlamydospora*: changes in phenolic production, oxidative state and expression of defence-related genes. *Eur. J. Plant Pathol.* 132, 133–146. doi:10.1007/s10658-011-9857-4.

Liu, S. li, Wu, J., Zhang, P., Hasi, G., Huang, Y., Lu, J., et al. (2016). Response of phytohormones

and correlation of SAR signal pathway genes to the different resistance levels of grapevine against *Plasmopara viticola* infection. *Plant Physiol. Biochem.* 107, 56–66. doi:10.1016/J.PLAPHY.2016.05.020.

Lorena, T., Calamassi, R., Mori, B., Mugnai, L., and Surico, G. (2001). *Phaeomoniella*

*chlamydospora*-grapevine interaction: Histochemical reactions to fungal infection. *Phytopathol. Mediterr.* 40, 400–406. doi:10.1400/14656.

Magnin-Robert, M., Adrian, M., Trouvelot, S., Spagnolo, A., Jacquens, L., Letousey, P., et al.

(2017). Alterations in Grapevine Leaf Metabolism Occur Prior to Esca Apoplexy Appearance. *Mol. Plant-Microbe Interact.* 30, 946–959. doi:10.1094/MPMI-02-17-0036-R.

Martin, M. (2011). Cutadapt removes adapter sequences from high-throughput sequencing

reads. *EMBnet.journal* 17, 10–12. doi:10.14806/EJ.17.1.200.

Massonnet, M., Figueroa-Balderas, R., Galarneau, E. R. A. A., Miki, S., Lawrence, D. P., Sun, Q., et al. (2017). Neofusicoccum parvum Colonization of the Grapevine Woody Stem Triggers Asynchronous Host Responses at the Site of Infection and in the Leaves. *Front. Plant Sci.* 8, 1117. doi:10.3389/fpls.2017.01117.

Mauch-Mani, B., and Mauch, F. (2005). The role of abscisic acid in plant–pathogen interactions. *Curr. Opin. Plant Biol.* 8, 409–414. doi:10.1016/J.PBI.2005.05.015.

McHale, L., Tan, X., Koehl, P., and Michelmore, R. W. (2006). Plant NBS-LRR proteins: Adaptable guards. *Genome Biol.* 7, 1–11. doi:10.1186/GB-2006-7-4-212/FIGURES/5.

Mondello, V., Larignon, P., Armengol, J., Kortekamp, A., Vaczy, K., Prezman, F., et al. (2018). Management of grapevine trunk diseases: Knowledge transfer, current strategies and innovative strategies adopted in Europe. *Phytopathol. Mediterr.* 57, 369–383. doi:10.14601/Phytopathol\_Mediterr-23942.

Munkvold, G. P., and Marois, J. J. (1995). Factors associated with variation in susceptibility of grapevine pruning wounds to infection by *Eutypa lata*. *Phytopathology* 85, 249–256. doi:10.1094/PHYTO-85-249.

Pérez-Donoso, A. G., Greve, L. C., Walton, J. H., Shackel, K. A., and Labavitch, J. M. (2007). *Xylella fastidiosa* Infection and Ethylene Exposure Result in Xylem and Water Movement Disruption in Grapevine Shoots. *Plant Physiol.* 143, 1024–1036. doi:10.1104/PP.106.087023.

Pierron, R., Gorfer, M., Berger, H., Jacques, A., Sessitsch, A., Strauss, J., et al. (2015a).

- Deciphering the Niches of Colonisation of *Vitis vinifera* L. by the Esca-Associated Fungus *Phaeoacremonium aleophilum* Using a gfp Marked Strain and Cutting Systems. *PLoS One* 10, e0126851. doi:10.1371/journal.pone.0126851.
- Pierron, R. J. G., Pages, M., Couderc, C., Compant, S., Jacques, A., and Violleau, F. (2015b). In vitro and in planta fungicide properties of ozonated water against the esca-associated fungus *Phaeoacremonium aleophilum*. *Sci. Hortic. (Amsterdam)*. 189, 184–191. doi:10.1016/j.scienta.2015.03.038.
- Pierron, R. J. G., Pouzoulet, J., Couderc, C., Judic, E., Compant, S., and Jacques, A. (2016). Variations in Early Response of Grapevine Wood Depending on Wound and Inoculation Combinations with *Phaeoacremonium aleophilum* and *Phaeomoniella chlamydospora*. *Front. Plant Sci.* 7, 1–14. doi:10.3389/fpls.2016.00268.
- Pieterse, C. M. J., Van Der Does, D., Zamioudis, C., Leon-Reyes, A., and Van Wees, S. C. M. (2012). Hormonal Modulation of Plant Immunity. <http://dx.doi.org/10.1146/annurev-cellbio-092910-154055> 28, 489–521. doi:10.1146/ANNUREV-CELLBIO-092910-154055.
- Pouzoulet, J., Mailhac, N., Couderc, C., Besson, X., Daydé, J., Lummerzheim, M., et al. (2013). A method to detect and quantify *Phaeomoniella chlamydospora* and *Phaeoacremonium aleophilum* DNA in grapevine-wood samples. *Appl. Microbiol. Biotechnol.* 97, 10163–10175. doi:10.1007/s00253-013-5299-6.
- Robert-Seilaniantz, A., Grant, M., and Jones, J. D. G. (2011). Hormone crosstalk in plant disease and defense: more than just jasmonate-salicylate antagonism. *Annu. Rev. Phytopathol.* 49, 317–343. doi:10.1146/ANNUREV-PHYTO-073009-114447.

- Romeo-Oliván, A., Chervin, J., Breton, C., Lagravère, T., Daydé, J., Dumas, B., et al. (2022). Comparative Transcriptomics Suggests Early Modifications by Vintec® in Grapevine Trunk of Hormonal Signaling and Secondary Metabolism Biosynthesis in Response to *Phaeoconiella chlamydospora* and *Phaeoacremonium minimum*. *Front. Microbiol.* 13.
- Romeo-Oliván, A., Pagès, M., Breton, C., Lagarde, F., Cros, H., Yobrégat, O., et al. (2021). Ozone Dissolved in Water: An Innovative Tool for the Production of Young Plants in Grapevine Nurseries? *Ozone Sci. Eng.* doi:10.1080/01919512.2021.1984203.
- Samanta, A., Das, G., and Das, S. (2011). Roles of flavonoids in plants. *Carbon N. Y.* 100, 6. Available at: [https://www.researchgate.net/publication/279499208\\_Roles\\_of\\_flavonoids\\_in\\_Plants](https://www.researchgate.net/publication/279499208_Roles_of_flavonoids_in_Plants).
- Shah, A., and Smith, D. L. (2020). Flavonoids in agriculture: Chemistry and roles in, biotic and abiotic stress responses, and microbial associations. *Agronomy* 10. doi:10.3390/AGRONOMY10081209.
- Shigo, A., and Marx, H. (1977). Compartmentalization of decay in trees. Available at: [https://books.google.com/books?hl=es&lr=&id=ut9q7fQsWtIC&oi=fnd&pg=PA1&ots=Ei8Bc9dhU-&sig=1eAAiKxWCiC-Bs\\_1ONNYE-STd4A](https://books.google.com/books?hl=es&lr=&id=ut9q7fQsWtIC&oi=fnd&pg=PA1&ots=Ei8Bc9dhU-&sig=1eAAiKxWCiC-Bs_1ONNYE-STd4A).
- Spagnolo, A., Magnin-Robert, M., Alayi, T. D., Cilindre, C., Mercier, L., Schaeffer-Reiss, C., et al. (2012). Physiological changes in green stems of *Vitis vinifera* L. cv. Chardonnay in response to esca proper and apoplexy revealed by proteomic and transcriptomic analyses. *J. Proteome Res.* 11, 461–475. doi:10.1021/pr200892g.
- Stempien, E., Goddard, M.-L. L., Leva, Y., Bénard-Gellon, M., Laloue, H., Farine, S., et al. (2018).

- Secreted proteins produced by fungi associated with *Botryosphaeria dieback* trigger distinct defense responses in *Vitis vinifera* and *Vitis rupestris* cells. *Protoplasma* 255, 613–628. doi:10.1007/S00709-017-1175-Z/FIGURES/7.
- Sumner, L. W., Amberg, A., Barrett, D., Beale, M. H., Beger, R., Daykin, C. A., et al. (2007). Proposed minimum reporting standards for chemical analysis. *Metabolomics* 3, 211–221. doi:10.1007/s11306-007-0082-2.
- Ton, J., Flors, V., and Mauch-Mani, B. (2009). The multifaceted role of ABA in disease resistance. *Trends Plant Sci.* 14, 310–317. doi:10.1016/J.TPLANTS.2009.03.006.
- Tsugawa, H., Cajka, T., Kind, T., Ma, Y., Higgins, B., Ikeda, K., et al. (2015). MS-DIAL: data-independent MS/MS deconvolution for comprehensive metabolome analysis. *Nat. Methods* 2015 126 12, 523–526. doi:10.1038/nmeth.3393.
- Tsugawa, H., Kind, T., Nakabayashi, R., Yukihiro, D., Tanaka, W., Cajka, T., et al. (2016). Hydrogen Rearrangement Rules: Computational MS/MS Fragmentation and Structure Elucidation Using MS-FINDER Software. *Anal. Chem.* 88, 7946–7958. doi:10.1021/ACS.ANALCHEM.6B00770/SUPPL\_FILE/AC6B00770\_SI\_013.XLSX.
- Tuladhar, P., Sasidharan, S., and Saudagar, P. (2021). Role of phenols and polyphenols in plant defense response to biotic and abiotic stresses. *Biocontrol Agents Second. Metab.*, 419–441. doi:10.1016/B978-0-12-822919-4.00017-X.
- Vallad, G. E., and Goodman, R. M. (2004). Systemic Acquired Resistance and Induced Systemic Resistance in Conventional Agriculture. *Crop Sci.* 44, 1920–1934. doi:10.2135/CROPSCI2004.1920.

- Wiklund, S., Johansson, E., Sjöström, L., Mellerowicz, E. J., Edlund, U., Shockcor, J. P., et al. (2008). Visualization of GC/TOF-MS-Based Metabolomics Data for Identification of Biochemically Interesting Compounds Using OPLS Class Models. *Anal. Chem.* 80 (1), 115–122. Available at: <https://doi.org/10.1021/ac0713510>.
- Yoshida, T., Christmann, A., Yamaguchi-Shinozaki, K., Grill, E., and Fernie, A. R. (2019). Revisiting the Basal Role of ABA – Roles Outside of Stress. *Trends Plant Sci.* 24, 625–635. doi:10.1016/J.TPLANTS.2019.04.008.

## Tables

**Table 1.** List of primers for q PCR (fungal detection).

Target	Sequence	Reference
$\beta$ -tubulin	Fw 5'- CGGTGGGGTTTTTACGTCTACAG -3'	Pouzoulet <i>et al.</i> (2013)
<i>P. minimum</i>	Rv 5'- CGTCATCCAAGATGCCGAATAAAG -3'	
$\beta$ -tubulin	Fw 5'- CTCTGGTGTGTAAGTTCAATCGACTC -3'	Pouzoulet <i>et al.</i> (2013)
<i>P. chlamydospora</i>	Rv 5'- CCATTGTAGCTGTTCCAAGATCAG -3'	

**Table 2.** Summary of characteristic markers in the tested conditions.

N°	m/z	RT (min)	Molecular Formula	Error (ppm)	Level of annotation	Chemical class <sup>c</sup>	Putative annotation	Major concerned treatment
1	120.08083	5.129	C <sub>8</sub> H <sub>9</sub> N	0.4497	generic	Indole	Indoline <sup>e</sup>	INi
2	225.05496 a	10.61 4	C <sub>14</sub> H <sub>10</sub> O <sub>4</sub>	1.5063	-	-	Unknown compound	IPch – IPm
3	229.08612	11.73 3	C <sub>14</sub> H <sub>12</sub> O <sub>3</sub>	0.8687	<i>Vitis</i>	Stilbenoid	Trans-resveratrol <sup>d</sup>	IPch – IPm
4	237.14857	18.17 8	C <sub>14</sub> H <sub>20</sub> O <sub>3</sub>	0.2066	generic	Benzoic acid	4-Hydroxybenzoic acid; Heptyl ether <sup>e</sup>	IPm
5	243.10197	14.14 6	C <sub>15</sub> H <sub>14</sub> O <sub>3</sub>	1.6413	<i>Vitis</i>	Stilbenoid	Pinostilbene <sup>d</sup>	IPm
6	289.16507	9.636	C <sub>14</sub> H <sub>24</sub> O <sub>6</sub>	1.7464	-	Flavonoid <sup>f</sup>	Unknown compounds	IPm

7	318.30054	15.77 7	$C_{18}H_{39}NO_3$	0.85114	<i>Vitis</i>	Amine	4-hydroxysphinganine	IPch
8	379.15829	6.632	$C_{16}H_{26}O_{10}$	4.1750	-	-	Unknown compound	INi
9	393.12122	13.78 1	$C_{16}H_{24}O_9S$	0.4045	-	-	Unknown compound	IPch
10	406.24368	17.68 4	$C_{20}H_{31}N_5O_4$	2.9563	-	-	Unknown compound	IPch – IPm
11	435.12921	7.962	$C_{21}H_{22}O_{10}$	1.4639	<i>Vitis</i>	Flavonoid	3,3',4',7-Tetrahydroxyflavanone; 7-O-β-L-Rhamnopyranoside	IPch – IPm
12	455.14908	13.50 2	$C_{28}H_{22}O_6$	0.3625	<i>Vitis</i>	Stilbenoid	Ampelopsin D	IPch – IPm
13	493.62653 b	12.22 2	$C_{31}H_{58}O_{37}$	1.7908	-	Stilbenoid <sup>f</sup>	Unknown compound	INi
14	520.33997	17.76 5	$C_{26}H_{50}NO_7P$	0.3921	generic	Glycerophospholipid	LysoPC(18:2(9Z, 12Z)) <sup>e</sup>	IPch – IPm

15	535.19635	16.87 3	C <sub>30</sub> H <sub>30</sub> O <sub>9</sub>	0.1700	-	Flavonoid <sup>f</sup>	Unknown compound	IPm
16	575.17004	13.46 1	C <sub>35</sub> H <sub>26</sub> O <sub>8</sub>	0.0070	<i>Vitis</i>	Stilbenoid	Viniferal	INi
17	593.12939	9.625	C <sub>30</sub> H <sub>24</sub> O <sub>13</sub>	0.7132	<i>Vitis</i>	Flavonoid	Procyanidin A1 derivative	IPch – IPm
18	593.13019	9.23	C <sub>30</sub> H <sub>24</sub> O <sub>13</sub>	2.0619	<i>Vitis</i>	Flavonoid	Procyanidin A1 derivative	IPch – IPm
19	609.12451	8.311	C <sub>30</sub> H <sub>24</sub> O <sub>14</sub>	1.0310	<i>Vitis</i>	Flavonoid	Apigenin 7-glycosides; 7-O-[3,4-Dihydroxy-E-cinnamoyl-(→4)-β-D-glucuronopyranoside]	IPch – IPm
20	639.22302	16.65 3	C <sub>37</sub> H <sub>34</sub> O <sub>10</sub>	0.8542	-	Flavonoid <sup>f</sup>	Unknown compound	IPm
21	639.22308	16.27 9	C <sub>37</sub> H <sub>34</sub> O <sub>10</sub>	0.9480	generic	Flavonoid	3-benzoyl-5,5',6',7,7',8,8'-heptamethoxy-2'-phenyl-2,4'-spirobi[chromene]	IPm
22	669.23322	16.82 5	C <sub>38</sub> H <sub>36</sub> O <sub>11</sub>	0.2720	-	Flavonoid <sup>f</sup>	Unknown compound	IPm

23	669.23364	16.33 8	$C_{38}H_{36}O_{11}$	0.8995	-	Flavonoid <sup>f</sup>	Unknown compound	IPm
24	681.21204	13.78	$C_{42}H_{32}O_9$	0.1923	<i>Vitis</i>	Stilbenoid	Diptoindonesin B derivative (resveratrol trimer)	IPch
25	681.21222	13.32 5	$C_{42}H_{32}O_9$	0.4565	<i>Vitis</i>	Stilbenoid	Diptoindonesin B derivative (resveratrol trimer)	IPch
26	681.21228	13.17 6	$C_{42}H_{32}O_9$	0.5446	<i>Vitis</i>	Stilbenoid	Diptoindonesin B derivative (resveratrol trimer)	IPch
27	709.2265	16.48 5	$C_{40}H_{36}O_{12}$	2.0487	-	-	Unknown compound	IPm
28	745.1405	10.03 4	$C_{37}H_{28}O_{17}$	0.7703	<i>Vitis</i>	Flavonoid	3,3',4',5,5',7-Hexahydroxyflavan- (2→7,4→8)-3,3',4',5,7- pentahydroxyflavan; 3'-O-(3,4,5- Trihydroxybenzoyl)	IPch – IPm

29	783.26196	17.20 9	C <sub>49</sub> H <sub>39</sub> N <sub>2</sub> O <sub>6</sub> P	0.1404	-	Glycerophospholip ids <sup>f</sup>	Unknown compound	IPm
30	881.19281	8.985	C <sub>45</sub> H <sub>36</sub> O <sub>19</sub>	0.5163	<i>Vitis</i>	Flavonoid	5,13-bis(3,4-dihydroxyphenyl)-7-[3,5,7-trihydroxy-2-(3,4,5-trihydroxyphenyl)-3,4-dihydro-2H-1-benzopyran-8-yl]-4,12,14-trioxapentacyclo[11.7.1.0 <sup>2</sup> , <sup>11</sup> .0 <sup>3</sup> , <sup>8</sup> .0 <sup>15</sup> , <sup>20</sup> ]h enicoso-2(11),3(8),9,15,17,19-hexaene-6,9,17,19,21-pentol	IPch – IPm
31	921.25421	14.29 6	C <sub>56</sub> H <sub>40</sub> O <sub>13</sub>	0.0456	<i>Vitis</i>	Stilbenoid	Amurensin K	INi

<sup>a</sup> [M+H-H<sub>2</sub>O]<sup>+</sup>

<sup>b</sup> [M+H-2H<sub>2</sub>O]<sup>2+</sup>

<sup>c</sup> Determined with ClassyFire .

### Figure captions

**Figure 1.** Fungal trunk colonization expressed as the number of fungal  $\beta$ -tubulin gene copies per mg of wood six weeks post-infection. INi (Pm) = Injured control, challenged with primers targeting the *P. minimum*  $\beta$ -tubulin gene; INi (Pch) = Injured control, challenged with primers targeting the *P. chlamydospora*  $\beta$ -tubulin gene; IPm = Samples infected with *P. minimum*, challenged with primers targeting the *P. minimum*  $\beta$ -tubulin gene; IPch = Samples infected with *P. chlamydospora*, challenged with primers targeting the *P. chlamydospora*  $\beta$ -tubulin gene. Asterisks indicate significant differences between conditions (p-value < 0.001 \*\*, <0.00001 \*\*\*\*). N = 9.

**Figure 2.** (A) Number of differentially expressed genes (DEGs) per condition (injury, INi; *P. minimum*, IPm; *P. chlamydospora*, IPch), indicating specific and overlapping DEGs. The term “overlapping” refers to genes that are differentially regulated both by the injury and the pathogen. (B) Venn diagram showing DEGs specifically upregulated or downregulated by each or both pathogens. (C) Functional enriched subcategories among DEGs up- and down-regulated by *P. minimum* (dark yellow, UP; light yellow, DOWN) or *P. chlamydospora* (dark blue, UP; light grey, DOWN). The size of the circle represents the number of DEGs associated with each category. Fisher’s test, p-value < 0.05

**Figure 3.** (A) Gene hierarchical tree together with assigned modules. Each vertical line corresponds to one gene. Modules are represented by colors. (B) Hierarchical relationships between gene co-expression modules. (C) Heatmap representing the log<sub>2</sub> expression value of each module eigengene per biological condition. Each row represents the module eigengene expression, each column represents the biological condition (NINi = non-injured and non-

infected control; INi = injured but non-infected control; IPm = injured and infected with *P. minimum*; IPch = Injured and infected with *P. chlamydospora*). The module eigengene represents the principal component of the variability in the module gene expression and can be interpreted as an average of the module's gene expression profile. Blue-White-Red color key indicates the log<sub>2</sub> gene expression value. (D) Heatmaps representing gene expression profiles of all the genes in each module. Each row represents one gene, each column represents the biological condition (NINi = non-injured and non-infected control; INi = injured but non-infected control; IPm = injured and infected with *P. minimum*; IPch = Injured and infected with *P. chlamydospora*). The numbers appearing on the right of each heatmap indicate different gene clusters. Modules are represented by colors. Blue-White-Red color key indicates the log<sub>2</sub> gene expression value.

**Figure 4.** PCA score plot of ESI-PI data from *Vitis* wood extract. Colored circles arbitrarily enclose treatment types: Injured/Not inoculated (INi) samples; Injured/ *P. chlamydospora* (IPch) and Injured + *P. minimum* (IPm); Quality control (QC).

**Figure 5.** Shared and unique (SUS) plot highlights the most significant features that change according to wood treatment. X-axis: compounds in higher abundance in control samples (INi, left, black triangle) or in samples inoculated with *P. minimum* (IPm, right, yellow triangle). Y-axis: compounds in higher abundance in control samples (INi, down, black triangle) or in samples inoculated with *P. chlamydospora* (IPch, up, blue triangle). Purple triangle in the upper-right square displayed common features to IPch and IPm.

**Figure 6.** Heatmap of the putative markers. The color key is based on average peak intensity of each feature by class: red color for higher peak intensity and blue color for lower peak intensity. Injured/Not inoculated (INi); Injured/ *P. chlamydospora* (IPch) and Injured/ *P. minimum* (IPm). Report to Table 2 for metabolite annotation.

**Figure 7.** Mass spectral similarity network of putative markers based on ESI-PI dataset of UHPLC-HRMS. Putative structures were based on HRMS and MS/MS spectra. Color tag is based on chemical class determined with ClassyFire. Node size of markers was arbitrarily increased (A). Highlight of markers overproduced in INi (B), IPch (C) and IPm (D), based on OPLS-DA coefficients. Highest values correspond to biggest nodes whereas the lowest correspond to smallest nodes.

**Figure S1.** Whole dataset heatmap. The color key is based on average peak intensity of each feature by class: red color for higher peak intensity and blue color for lower peak intensity. Injured/Not inoculated (INi); Injured/ *P. chlamydospora* (IPch) and Injured/ *P. minimum* (IPm).



1

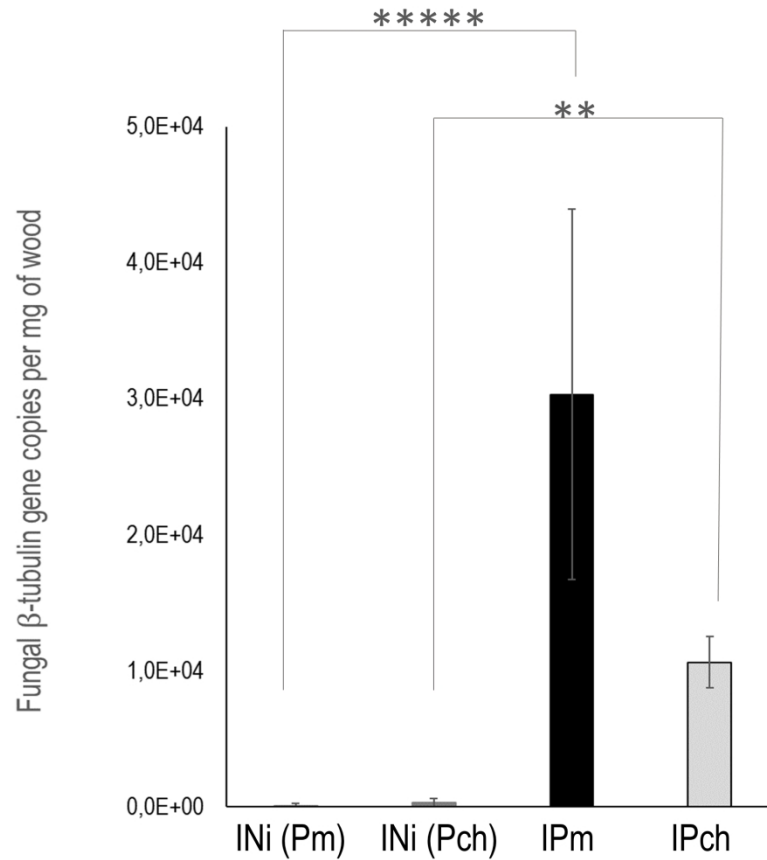


Figure. 1. Fungal trunk colonization expressed as the number of fungal  $\beta$ -tubulin gene copies per mg of wood six weeks post-infection. INi (Pm) = Injured control, challenged with primers targeting the *P. minimum*  $\beta$ -tubulin gene; INi (Pch) = Injured control, challenged with primers targeting the *P. chlamydospora*  $\beta$ -tubulin gene; IPm = Samples infected with *P. minimum*, challenged with primers targeting the *P. minimum*  $\beta$ -tubulin gene; IPch = Samples infected with *P. chlamydospora*, challenged with primers targeting the *P. chlamydospora*  $\beta$ -tubulin gene. Asterisks indicate significant differences between conditions (p-value < 0.001 \*\*, <0.00001 \*\*\*\*). N = 9.

600x600mm (96 x 96 DPI)

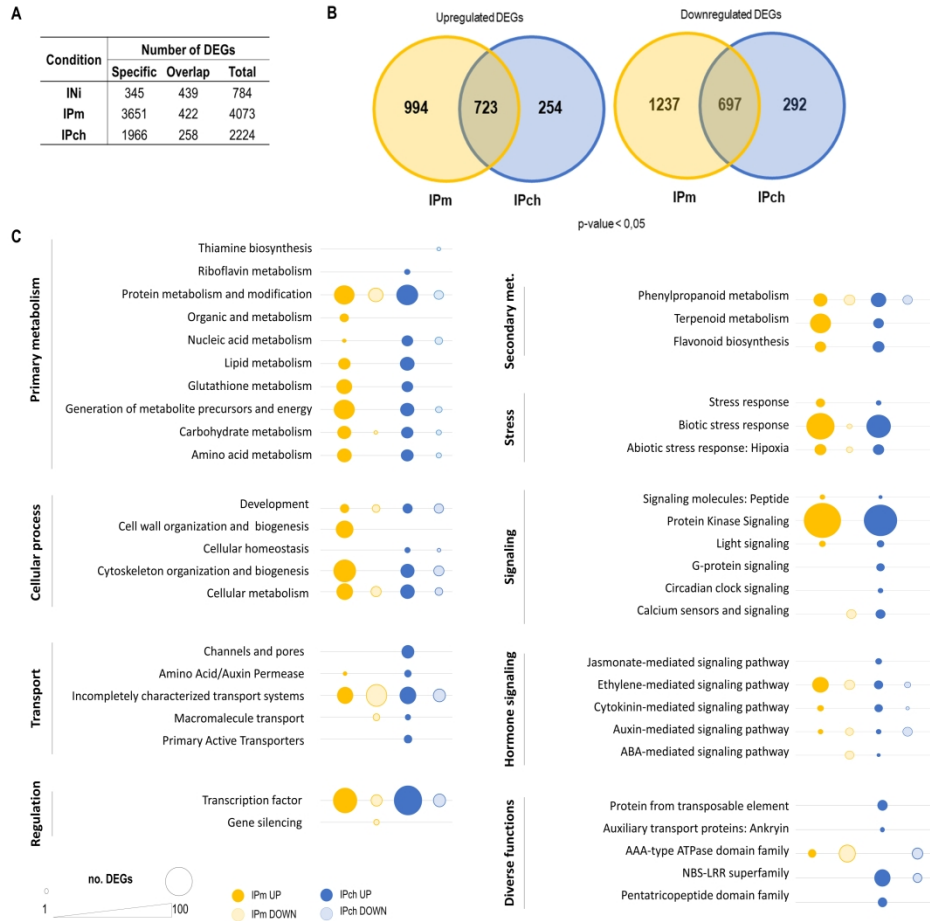


Figure 2. (A) Number of differentially expressed genes (DEGs) per condition (injury, INi; P. minimum, IPm; P. chlamydospora, IPch), indicating specific and overlapping DEGs. The term “overlapping” refers to genes that are differentially regulated both by the injury and the pathogen. (B) Venn diagram showing DEGs specifically upregulated or downregulated by each or both pathogens. (C) Functional enriched subcategories among DEGs up- and down- regulated by P. minimum (dark yellow, UP; light yellow, DOWN) or P. chlamydospora (dark blue, UP; light grey, DOWN). The size of the circle represents the number of DEGs associated to associated with each category. Fisher’s test, p-value < 0.05

821x788mm (150 x 150 DPI)

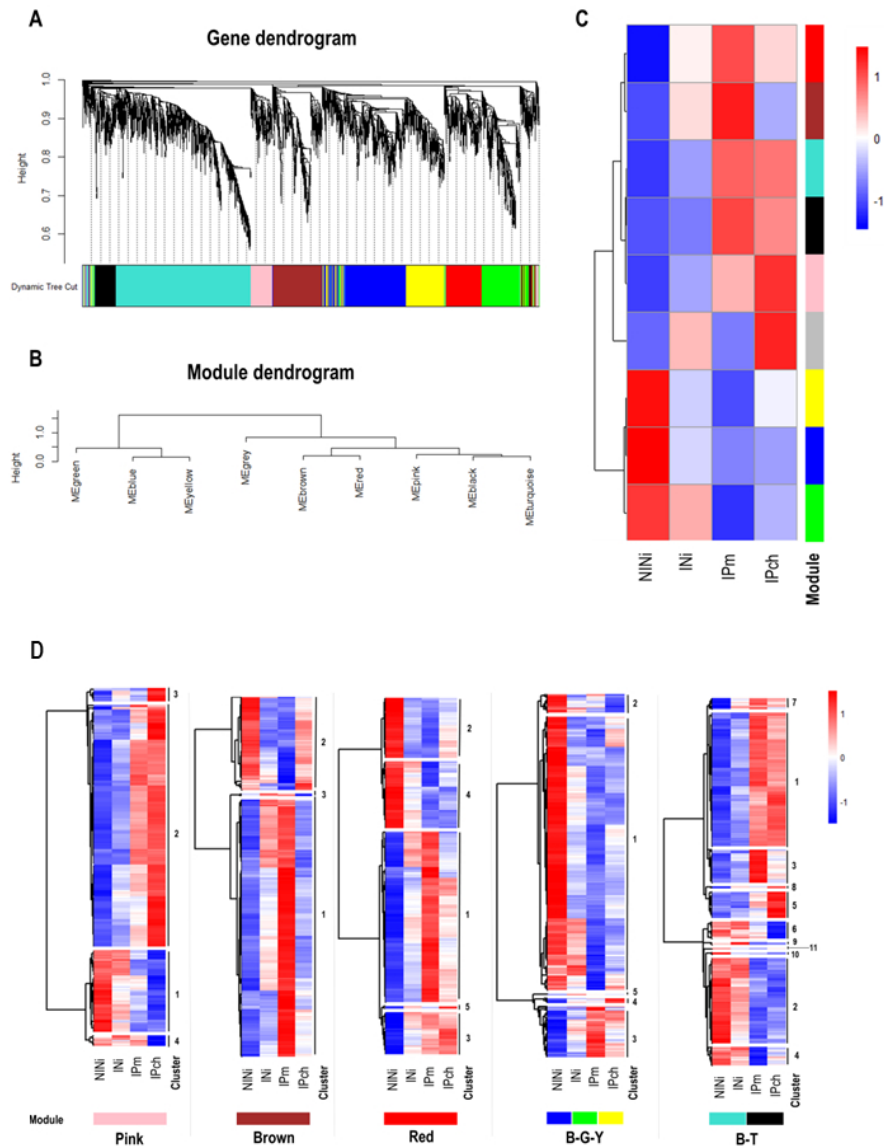


Figure 3. (A) Gene hierarchical tree together with assigned modules. Each vertical line corresponds to one gene. Modules are represented by colors. (B) Hierarchical relationships between gene co-expression modules. (C) Heatmap representing the  $\log_2$  expression value of each module eigengene per biological condition. Each row represents the module eigengene expression, each column represents the biological condition (NINi = non-injured and non-infected control; INi = injured but non-infected control; IPm = injured and infected with *P. minimum*; IPch = Injured and infected with *P. chlamydospora*). The module eigengene represents the principal component of the variability in the module gene expression and can be interpreted as an average of the module's gene expression profile. Blue-White-Red color key indicates the  $\log_2$  gene expression value. (D) Heatmaps representing gene expression profiles of all the genes in each module. Each row represents one gene, each column represents the biological condition (NINi = non-injured and non-infected control; INi = injured but non-infected control; IPm = injured and infected with *P. minimum*; IPch = Injured and infected with *P. chlamydospora*). The numbers appearing on the right of each heatmap indicate different gene clusters. Modules are represented by colors. Blue-White-Red color key indicates the  $\log_2$  gene expression value.

190x250mm (96 x 96 DPI)



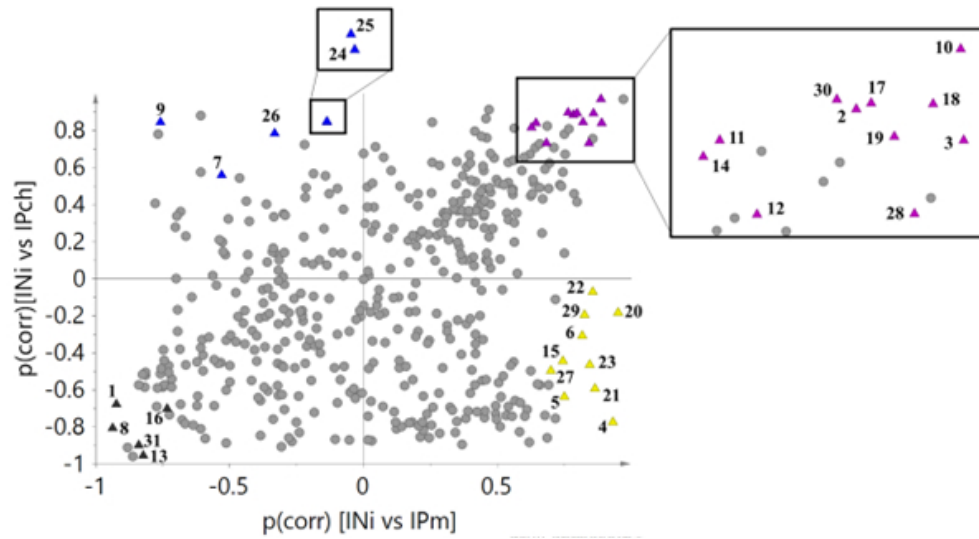


Figure 5. Shared and unique (SUS) plot highlights the most significant features that change according to wood treatment. X-axis: compounds in higher abundance in control samples (INi, left, black triangle) or in samples inoculated with *P. minimum* (IPm, right, yellow triangle). Y-axis: compounds in higher abundance in control samples (INi, down, black triangle) or in samples inoculated with *P. chlamyospora* (IPch, up, blue triangle). Purple triangle in the upper-right square displayed common features to IPch and IPm.

160x89mm (96 x 96 DPI)

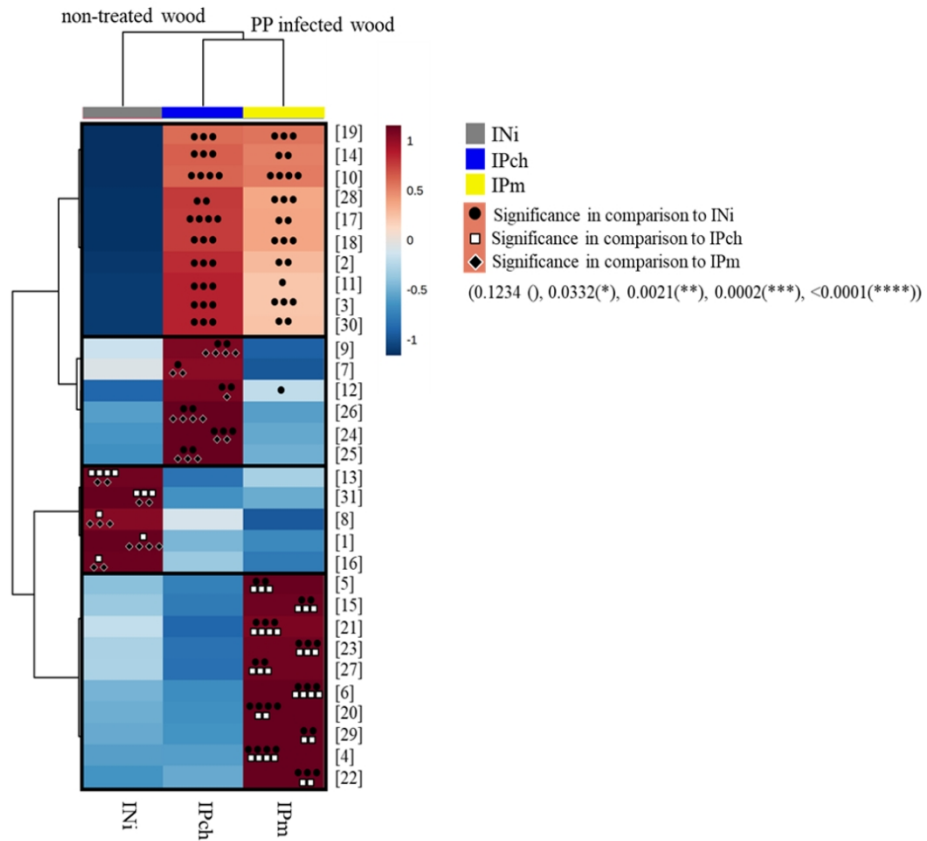


Figure 6. Heatmap of the putative markers. The color key is based on average peak intensity of each feature by class: red color for higher peak intensity and blue color for lower peak intensity. Injured/Not inoculated (INi); Injured/ *P. chlamydospora* (IPch) and Injured/ *P. minimum* (IPm). Report to Table 2 for metabolite annotation.

195x184mm (150 x 150 DPI)



Figure 7. Mass spectral similarity network of putative markers based on ESI-PI dataset of UHPLC-HRMS. Putative structures were based on HRMS and MS/MS spectra. Color tag is based on chemical class determined with ClassyFire. Node size of markers was arbitrarily increased (A). Highlight of markers overproduced in INi (B), IPch (C) and IPm (D), based on OPLS-DA coefficients. Highest values correspond to biggest nodes whereas the lowest correspond to smallest nodes.

159x101mm (96 x 96 DPI)



**Table S2.** Enriched functional categories among DEGs UP and DOWN-regulated during the infection with *P. minimum* or *P. chlamydospora*.

<b>Enriched functional categories among upregulated DEGs during the infection with <i>P. chlamydospora</i></b>		
<b>Functional Category</b>	<b>DEGs</b>	<b>p-value</b>
Transcription factor: WRKY family	17	2,20E-16
Biotic stress response: Plant-pathogen interaction (R-prot)	25	2,20E-16
Protein Kinase Signaling	82	2,20E-16
Primary amino acids derivated metabolism: Monoterpenoid metabolism	12	3,68E-13
NBS-LRR superfamily	13	4,70E-08
Glutathione metabolism	8	5,34E-07
Transcription factor: FAR1-like family.	5	1,84E-06
Light signaling	4	2,51E-06
Biotic stress response: Plant-pathogen interaction	9	4,54E-06
Protein metabolism and modification: Proteolysis	18	5,13E-06
Cell wall organization and biogenesis	12	7,64E-06
Macromolecule transport: Multidrug transport.Multidrug ABC transport	9	1,18E-05
Phenylpropanoid metabolism: Phenylpropanoid biosynthesis	8	1,43E-05
Oxidatio-reduction: Cytochrome P450 oxidoreductase	8	2,81E-05
Electrochemical Potential-driven Transporters: Porters.Drug/Metabolite Transporter	7	3,34E-05
Transcription factor: Zinc finger B-box family	3	6,53E-05
G-protein signaling	5	7,79E-05
Abiotic stress response: Wounding	3	1,03E-04
Transcription factor: SRS family	2	1,16E-04
Transcription factor: MYB family	6	1,26E-04
AAA-type ATPase domain family	4	1,64E-04
Lipid metabolism: Sphingolipid biosynthesis	2	2,31E-04
Calcium sensors and signaling	7	2,33E-04
Cytokinin inactivation	3	2,52E-04
Electrochemical Potential-driven Transporters: Major Facilitator Superfamily. Sugar Porter	4	2,70E-04
Biotic stress response: Plant-pathogen interaction (virus)	3	2,93E-04
Biotic stress response	7	3,54E-04
Lipid metabolism: Glycerolipid catabolism	3	3,86E-04
Carbohydrate metabolism: Glycosyl transference	4	4,78E-04
Electrochemical Potential-driven Transporters: Major Facilitator Superfamily. Nitrate/Nitrite Porter	2	5,72E-04
Protein from transposable element	5	1,03E-03
Ethylene-mediated signaling pathway	6	1,11E-03

Transcription factor: GRAS family.	3	1,35E-03
Primary amino acids derivated metabolism: Terpenoid biosynthesis (Carotenoids)	3	1,72E-03
Phenylpropanoid metabolism: Flavonoid biosynthesis (Anthocyanin)	4	1,76E-03
Protein metabolism and modification: Protein synthesis (Ribosome)	8	1,88E-03
Abiotic stress response: Oxidative stress	3	3,36E-03
Carbohydrate metabolism: Glycolisis Gluconeogenesis	5	3,84E-03
Cytokinin biosynthesis	2	3,86E-03
Auxiliary transport proteins: Ankyrin	4	4,90E-03
Phenylpropanoid metabolism: Flavonoid biosynthesis	4	5,40E-03
Auxin inactivation	2	5,55E-03
Generation of metabolite precursors and energy: Photosynthesis.Antenna proteins	2	5,55E-03
Transcription factor: TCP family	2	5,55E-03
Electrochemical Potential-driven Transporters: Porters. Monovalent Cation:Proton Antiporter-8	1	6,24E-03
Generation of metabolite precursors and energy: Photosynthesis.Reaction center pigment biosynthesis	1	6,24E-03
Incompletely characterized transport systems: Putative transport protein.YdjX-Z	1	6,24E-03
Transcription factor: AP2 family	1	6,24E-03
Jasmonate-mediated signaling pathway	3	6,60E-03
Phenylpropanoid metabolism: Flavonoid biosynthesis (Glycoside)	2	6,84E-03
Generation of metabolite precursors and energy: Storage proteins	4	7,48E-03
Lipid metabolism: Fatty acid metabolism.Alpha-linolenic acid metabolism	3	7,87E-03
Electrochemical Potential-driven Transporters: Porters. Oligopeptide Transporter	2	8,99E-03
Transcription factor: CCAAT family. HAP3-Type	2	8,99E-03
Transcription factor: NAC family	3	1,00E-02
Reproductive developpment	6	1,06E-02
Amino acid metabolism: Cysteine metabolism	2	1,14E-02
Primary amino acids derivated metabolism: Glucosinolate metabolism	2	1,23E-02
Abiotic stress response: UV	1	1,25E-02
Transcription factor: MED	1	1,25E-02
Amino acid metabolism: Alanine and aspartate metabolism	3	1,29E-02
Generation of metabolite precursors and energy: Photosynthesis.Photosystem II	2	1,80E-02
Riboflavin metabolism	2	1,80E-02
Carbohydrate metabolism: Starch catabolism inhibitor	1	1,86E-02
Nucleic acid metabolism: DNA metabolism	4	1,93E-02
Amino acid metabolism: Methionine metabolism	3	2,00E-02
Amino acid metabolism: Tyrosine metabolism	2	2,12E-02
Nucleic acid metabolism: nucleotide metabolism	4	2,34E-02
ABA biosynthesis	1	2,47E-02

Generation of metabolite precursors and energy: Photosynthesis.Photosynthetic-chain phosphorylation	2	2,71E-02
Amino acid derivative metabolism	2	2,83E-02
Cellular homeostasis: Redox	2	2,83E-02
Transcription factor: bZIP family	2	2,83E-02
Lipid metabolism: Steroid biosynthesis	3	2,96E-02
Stress response	2	2,96E-02
Abiotic stress response: Hipoxia	1	3,08E-02
Signaling molecules: peptide	1	3,08E-02
Transcription factor: AS2 family	2	3,09E-02
Incompletely characterized transport systems: Nuclear pore complex	2	3,35E-02
Generation of metabolite precursors and energy: Photosynthesis.Calvin cycle	1	3,69E-02
Macromolecule transport: Macromolecule transport.Heme prostetic groups trafficking	1	3,69E-02
Transcription factor: TAZ family	1	3,69E-02
Circadian clock signaling	2	3,76E-02
Esterase activity	2	4,19E-02
Abiotic stress response: Light	1	4,29E-02
Primary Active Transporters. P-dep Fe <sup>2+</sup> Transporter	1	4,29E-02
Lipid metabolism: Fatty acid biosynthesis	2	4,79E-02
Electrochemical Potential-driven Transporters: Porters.K <sup>+</sup> Transporter	1	4,88E-02
Methane metabolism	1	4,89E-02
Protein metabolism and modification: Protein synthesis (Translation)	3	4,91E-02

<b>Enriched functional categories among downregulated DEGs during the infection with <i>P. chlamydospora</i></b>		
<b>Functional Category</b>	<b>DEGs</b>	<b>p-value</b>
Primary amino acids derivated metabolism: Diterpenoid metabolism	4	5,64E-05
Electrochemical Potential-driven Transporters: Amino Acid/Auxin Permease	4	1,28E-04
Protein metabolism and modification: Protein folding	6	1,94E-04
Primary amino acids derivated metabolism: Terpenoid biosynthesis (Carotenoids)	3	3,10E-04
Cell wall organization and biogenesis	7	4,49E-04
Auxin-mediated signaling pathway	5	1,49E-03
Electrochemical Potential-driven Transporters: Porters.Drug/Metabolite Transporter	4	1,55E-03
Transcription factor: Trihelix family	2	4,22E-03
Oxidatio-reduction: Cytochrome P450 oxidoreductase	4	4,41E-03
Pentatricopeptide domain family	6	4,67E-03
Root development	2	5,49E-03
Transcription factor: G2-like family.	2	6,54E-03
Auxin transport	2	1,06E-02

Channels and pores: beta-barrel porins. Mitochondrial and plastid	1	1,38E-02
Transcription factor: HSF domain family.	1	1,72E-02
No hit	20	1,75E-02
Phenylpropanoid metabolism: Flavonoid biosynthesis (Isoflavonoid)	2	1,78E-02
Reproductive developpment	4	1,92E-02
NBS-LRR superfamily	4	1,94E-02
Cytokinin catabolism	1	2,06E-02
Nucleic acid metabolism: DNA metabolism.Non homologous end joining	1	2,06E-02
Nucleic acid metabolism: nucleotide metabolism	3	2,23E-02
Generation of metabolite precursors and energy: Electron transport. Respiratory-chain phosphorylation	3	2,58E-02
Electrochemical Potential-driven Transporters: Porters. Multi Antimicrobial Extrusion	2	2,59E-02
Ethylene-mediated signaling pathway	3	2,65E-02
Carbohydrate metabolism: N-glycan biosynthesis	2	2,66E-02
Cellular homeostasis: Heavy metal ion	1	2,74E-02
Transcription factor: CCT family.	1	2,74E-02
Channels and pores: A-Type channels. Ammonia Channel Transporter	1	3,07E-02
Transcription factor: Homeobox domain family.	2	3,22E-02
Thiamine biosynthesis	1	3,41E-02
Transcription factor: GRF family.	1	3,74E-02
Amino acid metabolism: Urea cycle	2	4,22E-02
Transcription factor: FHA-like family.	1	4,74E-02

<b>Enriched functional categories among upregulated DEGs during the infection with <i>P. minimum</i></b>		
<b>Functional Category</b>	<b>DEGs</b>	<b>p-value</b>
Protein Kinase Signaling	102	2,87E-14
Phenylpropanoid metabolism: Phenylpropanoid biosynthesis	32	4,73E-13
Abiotic stress response: Wounding	7	7,87E-07
Generation of metabolite precursors and energy: Photosynthesis.Antenna proteins	7	3,50E-06
Primary amino acids derivated metabolism: Monoterpenoid metabolism	14	1,17E-05
Pentatricopeptide domain family	3	2,55E-05
Glutathione metabolism	15	4,12E-05
Ethylene-mediated signaling pathway	20	5,67E-05
Cell wall organization and biogenesis	32	2,22E-04
Senescence	6	2,29E-04
Generation of metabolite precursors and energy: Photosynthesis.Photosystem II	7	2,78E-04
Nucleic acid metabolism: RNA metabolism. mRNA splicing	1	5,92E-04
Abiotic stress response: Hipoxia	3	6,03E-04

Transcription factor: WRKY family	8	1,48E-03
Biotic stress response	18	2,15E-03
Oxidatio-reduction: Cytochrome P450 oxidoreductase	17	2,22E-03
Amino acid metabolism: Tyrosine metabolism	6	2,83E-03
Protein metabolism and modification: Protein synthesis (Ribosome)	26	3,79E-03
Generation of metabolite precursors and energy: Storage proteins	12	3,91E-03
Organic acid metabolism: Propanoate metabolism	5	3,95E-03
Phenylpropanoid metabolism: Flavonoid biosynthesis (Anthocyanin)	9	5,49E-03
Lipid metabolism: Fatty acid biosynthesis	7	6,80E-03
Stress response	6	6,99E-03
Biotic stress response: Plant-pathogen interaction (virus)	4	8,88E-03
Biotic stress response: Plant-pathogen interaction	16	9,03E-03
Transcription factor: FAR1-like family.	5	9,54E-03
Transcription factor: Zinc finger B-box family	3	1,36E-02
Signaling molecules: peptide	2	1,48E-02
Transcription factor: MYB family	11	1,70E-02
Carbohydrate metabolism: Pentose glucuronate interconversion	6	1,73E-02
Amino acid metabolism: Glycine, serine and threonine metabolism	7	2,03E-02
Electrochemical Potential-driven Transporters: Major Facilitator Superfamily. Nitrate/Nitrite Porter	2	2,16E-02
Biotic stress response: Plant-pathogen interaction (R-prot)	20	2,19E-02
Transcription factor: NAC family	7	2,34E-02
Light signaling	3	2,43E-02
Carbohydrate metabolism: Amino sugar metabolism	6	2,81E-02
Cytoskeleton organization and biogenesis	19	3,28E-02
Electrochemical Potential-driven Transporters: Folate-Biopterin Transporter	2	3,82E-02
Electrochemical Potential-driven Transporters: Porters. Monovalent Cation:Proton Antiporter-4	1	4,01E-02
Generation of metabolite precursors and energy: Photosynthesis.Reaction center pigment biosynthesis	1	4,01E-02
Incompletely characterized transport systems: Putative transport protein. YdjX-Z	1	4,01E-02
Transcription factor: AP2 family	1	4,01E-02
Transcription factor: ULTRAPETALA1	1	4,01E-02
Electrochemical Potential-driven Transporters: Porters. Proton-dependent Oligopeptide Transporter	6	4,27E-02
Cytokinin inactivation	3	4,40E-02
Auxin activation	2	4,79E-02
Lipid metabolism: Synthesis and degradation of ketone bodies	2	4,79E-02

Electrochemical Potential-driven Transporters: Major Facilitator Superfamily. Sugar Porter	5	4,91E-02
Reproductive development	5	4,94E-02

<b>Enriched functional categories among downregulated DEGs during the infection with <i>P. minimum</i></b>		
<b>Functional Category</b>	<b>DEGs</b>	<b>p-value</b>
Electrochemical Potential-driven Transporters: Porters. Multi Antimicrobial Extrusion	9	1,23E-06
Electrochemical Potential-driven Transporters: Porters. Drug/Metabolite Transporter	10	5,91E-05
Auxin transport	5	5,35E-04
Root development	4	1,25E-03
Transcription factor: G2-like family.	4	1,76E-03
Primary amino acids derivated metabolism: Diterpenoid metabolism	5	1,99E-03
Channels and pores: A-Type channels. The Voltage-gated Ion Channel (K <sup>+</sup> )	3	2,27E-03
Primary amino acids derivated metabolism: Terpenoid biosynthesis (Carotenoids)	4	2,40E-03
Electrochemical Potential-driven Transporters: Porters. Sulfate Permease	3	4,65E-03
Electrochemical Potential-driven Transporters: Amino Acid/Auxin Permease	5	4,97E-03
ABA-mediated signaling pathway	6	5,14E-03
Ethylene-mediated signaling pathway	8	6,74E-03
Pentatricopeptide domain family	14	8,89E-03
Protein metabolism and modification: Protein folding	9	1,05E-02
Carbohydrate metabolism: Glycan catabolism	1	1,49E-02
Electrochemical Potential-driven Transporters: Porters. Monovalent Cation:Proton Antiporter-17	1	1,49E-02
Oxidatio-reduction: Cytochrome P450 oxidoreductase	7	2,48E-02
Gene silencing	2	2,60E-02
Calcium sensors and signaling	7	2,74E-02
Protein metabolism and modification: Proteolysis	5	2,81E-02
Transcription factor: Homeobox domain family.	4	3,29E-02
Abiotic stress response: Oxidative stress	3	3,46E-02
Biotic stress response: Plant-pathogen interaction (virus)	2	3,86E-02

**Table S3:** Common annotated features found in fungi and wood fingerprints

<b>m/z</b>	<b>Molecular Formula</b>	<b>Level of annotation</b>	<b>Putative annotation</b>
114.09149	C <sub>6</sub> H <sub>11</sub> NO	generic	Epsilon-caprolactam
120.08083	C <sub>8</sub> H <sub>9</sub> N	generic	indoline

123.04012	C <sub>7</sub> H <sub>6</sub> O <sub>2</sub>	Togniaciaceae	salicylaldehyde
130.06503	C <sub>9</sub> H <sub>7</sub> N	generic	Quinoline
136.07579	C <sub>5</sub> H <sub>5</sub> N <sub>5</sub>	generic	Adenine
191.17969	C <sub>14</sub> H <sub>22</sub>	generic	Senedigitalene
192.1022	C <sub>11</sub> H <sub>13</sub> NO <sub>2</sub>	generic	Streptopyrrolidine
219.17465	C <sub>15</sub> H <sub>22</sub> O	generic	Zerumbone
237.14857	C <sub>14</sub> H <sub>20</sub> O <sub>3</sub>	Togniaciaceae	4-Hydroxybenzoic acid; Heptyl ether
279.19336	C <sub>13</sub> H <sub>22</sub> N <sub>6</sub> O	generic	CNP0433214
337.27368	C <sub>21</sub> H <sub>36</sub> O <sub>3</sub>	generic	3-alpha-hydroxycativalic acid methyl ester
361.31046	C <sub>24</sub> H <sub>40</sub> O <sub>2</sub>	generic	aglaiabbreviatin C
373.25888	C <sub>20</sub> H <sub>36</sub> O <sub>6</sub>	generic	thromboxane B1
379.32101*	C <sub>24</sub> H <sub>44</sub> O <sub>4</sub>	generic	UNPD188556
397.33151	C <sub>24</sub> H <sub>44</sub> O <sub>4</sub>	generic	UNPD188556
476.27753	C <sub>23</sub> H <sub>42</sub> NO <sub>7</sub> P	generic	LysoPE(18:3(6Z,9Z,12Z)/0:0)
478.29285	C <sub>23</sub> H <sub>44</sub> NO <sub>7</sub> P	generic	LysoPE(18:2(9Z,12Z)/0:0)
518.32428	C <sub>26</sub> H <sub>48</sub> NO <sub>7</sub> P	generic	LysoPC(18:3(6Z,9Z,12Z))
520.33972	C <sub>26</sub> H <sub>50</sub> NO <sub>7</sub> P	generic	LysoPC(18:2(9Z,12Z))

\*[M+H-H<sub>2</sub>O]<sup>+</sup>

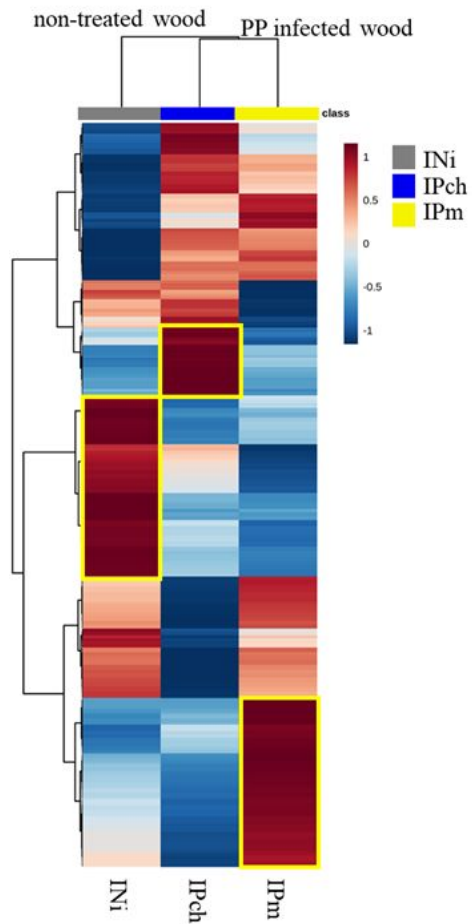


**Figure S1.** Whole dataset heatmap. The color key is based on average peak intensity of each feature by class: red color for higher peak intensity and blue color for lower peak intensity. Injured/Not inoculated (INi); Injured/ *P. chlamydospora* (IPch) and Injured/ *P. minimum* (IPm).